

Dynamic Coordinated MultiPoint (CoMP) Transmission Schemes

Master of Science Thesis in Communication Engineering

TILAK RAJESH LAKSHMANA

Department of Signals and Systems
Communication Systems Group
CHALMERS UNIVERSITY OF TECHNOLOGY
Göteborg, Sweden, 2010
Report No. EX015/2010

DYNAMIC COORDINATED MULTIPPOINT TRANSMISSION SCHEMES

Thesis for the degree of Master of Science



Front cover: An abstract representation of partial coordination between base stations. The base station's coverage area are of the same color denote an interference prone system with frequency reuse factor of one. The base stations are like puppets and the central unit (slanted cross) is depicted as the master of puppets. The thick lines to the base station express a strong control over them (for channel state information) while the dashed line signifies the user is virtually the real master of the system.

All rights reserved. This publication is protected by law in accordance with "Lagen om Upphovsrätt, 1960:729". No part of this publication may be reproduced, stored in a retrieval system, or transmitted, in any form or by any means, electronic, mechanical, photocopying, recording, or otherwise, without the prior permission of the author.

Copyright ©Tilak Rajesh Lakshmana, Göteborg 2010.

Abstract

In LTE-Advanced, Coordinated MultiPoint (CoMP) transmission is one of the techniques proposed to mitigate intercell interference, especially for cell-edge users. CoMP techniques are divided into coordinated beamforming/scheduling and joint processing. This thesis focuses on joint processing, where the user receives its data from various base stations, improving the signal strength and canceling interference. Coherent joint processing imposes perfect channel knowledge and perfect synchronization between base stations, but yields substantial theoretical gains. In the previous work, three joint processing approaches were studied in a static cluster of base stations for a flat fading Rayleigh channel. In the Centralized Joint Processing approach, global channel state information was available at the transmitter side, and the base stations within the cluster jointly performed the power allocation and the design of the beamformer. This puts tremendous requirements on backhauling. The Partial Joint Processing approach formed a set of base stations within a predefined threshold for transmission, reducing the requirements in backhauling and feedback from users. Finally, in the Distributed Joint Processing scheme, the power allocation and beamformers were locally calculated for every base station. In this thesis, the performance of these algorithms is evaluated in a multipath environment using the WINNER II channel model. The worst case scenario in terms of interference is considered where all the users are allocated in all the resource blocks. Hence, the joint processing schemes are applied in the frequency domain in every resource block. In particular, the performance of the Partial Joint Processing algorithm is improved with frequency adaptive thresholding compared to non-adaptive frequency thresholding. The threshold values for the Partial Joint Processing algorithm depend on the WINNER II channel model. The relative average number of active links with frequency adaptive thresholding is lesser compared to non-adaptive thresholding. Fewer active links translate to sparse channel matrices available at the central unit and poses problems to design the zero-forcing beamformer. A partial zero-forcing method performs better under these conditions. For adaptive thresholds greater than 20dB, there is multiuser interference and the performance of the Partial Joint Processing scheme degrades when moving towards the cell-edge. In addition, the channel correlation matrix suffers from rank deficiency. This is more prominent near the base station. Based on this, an algorithm is developed which defines cooperation areas over the cluster as to when the Partial Joint Processing scheme can be applied or fallback on the Centralized or Distributed Joint Processing.

Keywords: CoMP, Joint Processing, WINNER, MU-MIMO, Network MIMO, Precoding, Beamforming, Zero-Forcing, Partial Zero-Forcing

Contents

Abstract	iii
Contents	v
List of Figures	vii
List of Tables	ix
Preface	xi
Acknowledgments	xiii
Notation	xv
1 Introduction	1
1.1 Background	1
1.2 Coordination	2
1.2.1 Classification of Coordinated MultiPoint techniques	3
1.2.2 Obstacles	3
1.3 Scope of this thesis	5
1.4 Organization	5
2 Problem Formulation	7
2.1 System Model	7
2.2 WINNER II Channel Model	10
2.2.1 Antenna Patterns	11
2.2.2 The Grid Layout	11
2.2.3 Channel Generation	13
2.3 Joint Processing Algorithms	14
2.3.1 Centralized Joint Processing (CJP)	17
2.3.2 Distributed Joint Processing (DJP)	17
2.3.3 Partial Joint Processing (PJP)	17
2.4 Resource Block Allocation	18
2.5 Partial Zero-Forcing Beamforming	18
3 Simulation Results and Discussion	23
3.1 System Parameters	23
3.2 Power allocation	23
3.3 Active Set Threshold value for various WINNER scenarios	24

CONTENTS

3.4	The Sum-Rate	25
3.5	Impact of Active links in PJP scheme	28
3.6	Effect of rank deficient scaled channel correlation matrix	28
4	Conclusions and Future Work	33
4.1	Weighted Power allocation in every Resource Block.	33
4.2	Joint Processing for a set of OFDM carriers	34
4.3	Hybrid thresholding	34
4.4	A realistic measure of the effects of imperfect CSI with Time evolution feature in WINNER channel model	35
4.5	Support for multiple antennas at MS	35
4.6	Antenna type	35
4.7	Multi-WINNER scenario	35
	Publication	37
	Appendix	45
A	Interim results and more discussion	46
A.1	Base Station radiation pattern	46
A.2	Analysis of the active set threshold value	47
A.3	Sum-Rate plots of C1 and A2 WINNER scenarios	47
A.4	Rank deficiency in C1 and A2 WINNER scenarios	47
A.5	Cooperation Area for C1 and A2 WINNER scenarios	49
B	MATLAB details	55
B.1	Parallel Computing Toolbox	55
B.2	<i>deploytool</i>	56
B.3	How to efficiently run simulations on the Cluster (Single Core)	57
	Bibliography	59

List of Figures

1.1	a) Coordinated Scheduling or Coordinated Beamforming b) Joint Processing / Transmission.	4
2.1	Layout: The gray hexagon in the middle is the cluster area. The dashed lines are the cell-edge regions.	8
2.2	Radiation Pattern of the Antenna 1 of BS and the MS (Generated using WIM2).	12
2.3	Grid of positions over the cluster area. Position 27 corresponds to the cluster-center.	13
2.4	Layout: At the cluster-center (Position 27), 3 users are dropped along an ellipse. The red circles denote the BSs (Generated using WIM2).	14
2.5	A typical NLOS channel from one of the antennas of the BS to the mobile user at the cluster-center for a) B1-Urban micro-cell b) A2-Indoor to Outdoor c) C1-Suburban macro-cell and d) C2-Urban macro-cell.	16
2.6	a) $\mathbf{H}(\tau; t)$ for a WINNER B1 NLOS scenario b) $\mathbf{H}(f; t)$ after a 256-point FFT c) Resource block for a given subcarrier.	19
2.7	The complete Resource Block structure.	20
3.1	Average number of BS transmitting to a user for various WINNER scenarios (LOS & NLOS) when only pathloss and shadowing are considered.	25
3.2	Prior work: Average sum-rate per cell along the normalized distance from BS ₁	26
3.3	Average Sum-Rate per cell per RB for WINNER scenario B1 (NLOS) with 6 users, for non-adaptive frequency thresholding in PJP scheme.	27
3.4	Percentage gain in average sum-rate per cell per RB due to frequency adaptive thresholding over non-adaptive frequency thresholding along the normalized distance from BS ₁ for WINNER scenario B1.	27
3.5	Percentage gain in average sum-rate per cell per RB due to frequency adaptive thresholding over non-adaptive frequency thresholding along the normalized distance from BS ₁ for WINNER scenario C1.	28

LIST OF FIGURES

3.6	a) Average number of active links with non-adaptive frequency thresholding and frequency adaptive thresholding, b) Relative average number of active links of frequency adaptive thresholding versus non-adaptive frequency thresholding. Both figures are based on WINNER scenario B1.	29
3.7	Probability that the scaled channel correlation matrix is rank deficient for the non-adaptive frequency thresholding and frequency adaptive thresholding in WINNER B1 (NLOS) scenario.	30
3.8	Rank deficiency is more prominent closer to BS ₁ in non-adaptive frequency thresholding compared to frequency adaptive thresholding while it is vice-versa on the cell-edge in WINNER B1 (NLOS) scenario.	31
3.9	Cooperation Area for PJP-10dB for WINNER B1 (NLOS) scenario, a) frequency adaptive thresholding b) non-adaptive frequency thresholding.	32
4.1	Power allocation based on channel conditions in every subcarrier or RB.	34
A.1	Total Radiation pattern of a single BS with 3 antennas.	46
A.2	Average number of BS serving a user for various WINNER (NLOS) scenarios considering a) full channel, b) only pathloss and shadow fading c) only pathloss.	49
A.3	Difference in the average number of BS serving a user between full channel and channel with only pathloss and shadow fading.	50
A.4	WINNER Scenario C1 (NLOS) a) Average Sum-Rate per Cell per RB b) Percentage gain in average sum-rate per cell per RB due to Frequency adaptive thresholding compared to non-adaptive frequency thresholding.	51
A.5	WINNER Scenario A2 (NLOS), percentage gain in average sum-rate per cell per RB due to Frequency adaptive thresholding compared to non-adaptive frequency thresholding.	51
A.6	WINNER Scenarios (NLOS) a) C1, the rank deficiency is only prominent close to the BS and b) A2, the rank deficiency exists even for high thresholds.	52
A.7	Cooperation area for PJP-10dB for WINNER scenarios C1 (NLOS), a) frequency adaptive thresholding and b) non-adaptive frequency thresholding.	53
A.8	Cooperation area for PJP-10dB for WINNER scenarios A2 (NLOS), a) frequency adaptive thresholding and b) non-adaptive frequency thresholding.	54

List of Tables

3.1	Summary of System Parameters	24
A.1	MSE between the average number of BSs serving a user with full channel statistics and the channel with only pathloss and shadow fading for various WINNER scenarios	47
B.1	Summary of Execution Time	57

Preface

Apart from the actual thesis, this document can be considered as a quick tutorial for the starters who wish to get a good idea about joint processing with the WINNER Channel model. The main ideas are conveyed and are not completely reproduced from the original. The reader is encouraged to refer to the original journal/papers for their wonder. The reader is expected to know the wireless channel concepts to easily understand this material. For any questions regarding this material, the author can be contacted at tilak dot rajesh at gmail dot com.

This thesis is written using L^AT_EX and JabRef for bibliography. I hope you enjoy reading this report as much as I have enjoyed compiling it.

Acknowledgments

“Standing on the shoulders of giants”, everything is possible. I would like to thank my adviser Tommy Svensson for giving me this opportunity to work on CoMP. His deep insights about the WINNER channel model and prompt resolution of the obstacles that I faced, made this work, a pleasure. I would also like to thank Carmen Botella for her constant support during this work and in things concerning the department of Signals and Systems. She put things in such a way that it felt effortless. She constantly encouraged new ideas. The IEEE papers are always there but from my experience Carmen is the quickest reference. I admire them, simply for the fact that they are a step ahead of me. My heart felt gratitude to Tommy and Carmen for their invaluable suggestions and insightful discussions. They have taken good care of me during my thesis work at Chalmers.

I would also like to thank Nima Seifi for his prompt support in helping me to better understand the WINNER II channel model and answering my queries regarding the same. His licentiate was very helpful in understanding the bigger picture of CoMP. I have troubled a lot of people in making the simulations faster and bug free. In this regard, I would like to thank Andreas Bernsel of MathWorks Inc., for the seminar and support on parallel computing. Lassi Hentilä of Elektrobit for the prompt WINNER II bug support/clarification and many thanks to the C³SE folks especially Thomas Svedberg and Johan Landin, who answered every support query and even increased my home directory to 132GB. Lars Börjesson, a friendly system administrator was lightening quick to give me 1TB hard disk. I would also like to thank Madeleine Persson for installing the white board to scribble our vagrant thoughts and Agneta Kinnander for their help with the administrative process.

Special thanks to Erik Agrell et al. for inviting me for the CommSys workshop which really helped me in getting to know the team better and his notes on the minor details when it comes to technical writing [1]. This workshop involving the talks of Henk, Ali, Stylianos et al., who inspired me to write this report in Ly^X and use other open source software. This section would be incomplete without mentioning Erik Ström for everything he has done. The biweekly meetings would be incomplete without the tip of the day.

The times when I was working alone, I would like to thank Bob Dylan, The Beatles, Deep Purple, Charlie Parker for their brilliant music, that kept me more focused. Of course, thanks to Alex for Spotify without whose help this level of concentration might have been harder. The unforeseen breaks came mostly from one of the most cheerful person in the corridor, Guillermo, who always had a question and a new word for the day. I love these breaks. Navigating through more than 10,000 lines of code was easier with MATLAB command `>>` why.

Most of the time, I could identify more with Kalle than Hobbe, nonetheless, looking back it was a real calvinball time.

I would like to thank my family for their constant support and in making sure I ate healthy. I would also like to thank Kannan, Kamesh, Kasyab, Prakash, Peter, Uma, Arash, Eija, Johnny, Srikar, Yutao, Asif, Shajib, Kallol, Johan, Imad, Brita Lindsten, Patricia, Cédric, Barbara, Cecilia, Goutam, Srikanth, CNR, Vijay and Manu for their support in my times of joy and struggle.

There are many more friends and strangers who have gone out of their way to lend a helping hand, I thank them all.

Tilak Rajesh Lakshmana
Göteborg, 10th June, 2010

Notation

List of Symbols

\odot	Element-wise multiplication
\otimes	Kronecker product
$(\cdot)^{-1}$	Inverse
$(\cdot)^\dagger$	Moore-Penrose Pseudoinverse
$(\cdot)^H$	Hermitian (Complex Conjugate)
$(\cdot)^T$	Transpose
$\ \cdot\ $	Norm
$\ \cdot\ _F$	Frobenius Norm
a	Scalar (lower case letter)
\mathbf{a}	Vector (bold, lower case letter)
\mathbf{A}	Matrix (bold, upper case letter)
B_c	Coherence Bandwidth
$\mathbb{C}^{m \times n}$	Set of Complex valued $m \times n$ matrices
$\mathbb{E}_x[\cdot]$	Expectation operator w.r.t. x
$\mathcal{F}_x[\cdot]$	Discrete (Fast) Fourier Transform w.r.t. x
f_D	Doppler Frequency
K	Number of Base Stations
M	Number of Mobile Station
\mathbb{N}	Set of Natural numbers
N_T	Number of Antennas at Base Station
N_R	Number of Antennas at Mobile Station
$\mathbb{R}^{m \times n}$	Set of Real valued $m \times n$ matrices
T_C	Coherence Time
T_D	Delay Spread

Acronyms

2BS	2 Base Stations
3G,4G	3rd, 4th Generation
3GPP	3rd Generation Partnership Project
ACS	Array Coordinate System
AWGN	Additive White Gaussian Noise
BC	BroadCast
BF	BeamFormer
BS	Base Station/s
C ³ SE	Chalmers Centre for Computational Science and Engineering ¹
CoMP	Coordinated MultiPoint
CJP	Centralized Joint Processing
CSI	Channel State Information
CSIR	Channel State Information at the Receiver
CSIT	Channel State Information at the Transmitter
DFT	Discrete Fourier Transform
DJP	Distributed Joint Processing
DPC	Dirty Paper Coding
DL	DownLink
ECS	Element Coordinate System
FDD	Frequency Division Duplex
FFT	Fast Fourier Transform
GCS	Global Coordinate System
ICI	InterCell Interference
i.i.d.	Independent and Identically Distributed
IMT	International Mobile Telecommunications
ITU-R	International Telecommunication Union Radiocomm. Sector
JP	Joint Processing
LOS	Line of Sight

¹<http://www.c3se.chalmers.se/>

LTE	Long Term Evolution
MAC	Multiple Access Channel
MIMO	Multiple Input Multiple Output
MMSE	Minimum Mean Square Error
MRC	Maximum Ratio Combining
MS	Mobile Station
MSE	Mean Square Error
MU-MIMO	MultiUser MIMO
n -D	n Dimensional
NLOS	Non-Line of Sight
OFDM	Orthogonal Frequency Division Multiplexing
PJP	Partial Joint Processing
RB	Resource Block(s)
Rx	Receiver
SCM	Spatial Channel Model
SINR	Signal to Interference plus Noise Ratio
SNR	Signal to Noise Ratio
SR	Sum-Rate
SU-MIMO	Single User MIMO
TDD	Time Division Duplex
TR	Technical Report
Tx	Transmitter
UE	User Equipment
UCA	Uniform Circular Array
UL	Up-Link
ULA	Uniform Linear Array
WINNER	Wireless world INitiative NEW Radio
WIM2	WINNER II Channel Model
ZF	Zero Forcing

Chapter 1

Introduction

In recent past, Coordinated MultiPoint (CoMP) transmission has received much attention from the academia and the industry. This chapter motivates some of the reasons why this field is gaining so much attention. It also presents the classification and some of the obstacles faced in realizing CoMP schemes. This chapter concludes with the scope for this thesis and provides a layout of this document.

1.1 Background

The scarcity of bandwidth, spectrum and power in wireless systems has driven the need for spectrally efficient communication systems. The performance of a communication system is typically measured in terms of spectrum efficiency in bits/s/Hz/unit-area. In a cellular communication system such as 3GPP Long Term Evolution (LTE), the intercell interference is one of the main factors that influences the data rates of the users at the cell-edge and affects the average spectral efficiency of the cell.

When the frequencies of downlink transmission between neighboring cells are different, like in the conventional cellular systems, then the intercell interference will be a minor problem. This type of frequency reuse is common in older generation of wireless networks as it improves the Signal to Interference plus Noise Ratio (SINR). But the bandwidth available to reuse these frequencies is lower than the equivalent gain achieved with this SINR improvement [2]. Hence, conventional cellular systems suffer from poor spectral efficiency through high reuse factors. With a frequency reuse factor of one, as in LTE-Release 8, there will be interference between neighboring cells, especially at the cell-edge. Network coordination brings about choosing the antennas from different base stations (BSs) in suitable ways such that the interference is reduced and there is a tremendous increase in spectral efficiency attributed to the use of multiple antennas (Multiple Input Multiple Output-MIMO) at high Signal to Noise Ratio (SNR) [3]. Thus, coordination improves the user experience at the cell-edge, with exchange of information made possible via backhauling.

In the work of LTE-advanced, many advanced technologies have been considered. One such technology is CoMP where the main focus is on enhancing

the cell-edge user performance through coordinated beamforming/coordinated scheduling or joint processing. A consortium formed a project “EASY-C” for covering such conceptual research with field trials, aiming for low latency, fairness and high spectral efficiency. EASY-C is operating one of the world’s largest test beds and in June 2009, distributed CoMP was demonstrated in Dresden, Germany [4]. In January 2010, a new European research project, ARTIST4G was launched with the goal to explore further use of CoMP towards next generation wireless cellular systems.

1.2 Coordination

In a conventional cellular system, the BS is located in the cell center and it only serves the users in its coverage area. The signals transmitted from other BSs cause interference, especially at the cell-edge, where different coverage areas overlap, giving rise to InterCell Interference (ICI) which reduces the spectral efficiency of the cell. When the channel state information (CSI) of various links are made available to an entity (central unit) then the interference from other cells can be avoided by designing a beamformer. This pre-canceling of interference by beamforming and power allocation is called *Precoding*. Dirty Paper Coding (DPC) in this context can be viewed as a precoding technique which can completely remove the non-causally known interference at the transmitter in a Gaussian channel [5], i.e., pre-subtract the interference at the transmitter. In multiuser-MIMO, DPC is a capacity achieving technique but is not practically feasible, as it requires the CSI to be known noncausally at the transmitter. Hence, suboptimal beamforming techniques such as Zero Forcing Beamformer (ZFBF) or Minimum Mean Square Error (MMSE) beamformer can be used. ZFBF can asymptotically achieve the sum-rate that of DPC with efficient user selection [6]. The ZF when applied at the receiver eliminates interference but at the cost of increasing noise. When ZF is applied at the transmitter, it generally increases the average transmit power by the same factor [7]. Interference cancellation at the mobile station poses problems mainly due to the battery power and space constraint (e.g. more than two antennas at the user terminal), hence the interference cancellation needs to be carried out at the BS.

When a transmission to a user is collaborated by multiple BSs or network points, acting together to remove interference, this is referred to as CoMP transmission. For this to occur, the CSI from all the BSs needs to be available at the central unit for precoding. This constitutes the *centralized joint processing* algorithm, where a set of BSs form a cluster of cooperative cells. But, coordinating BSs for coherent joint processing puts tremendous requirements for high speed backhauling (10 Gbps over fiber or up to 4 Gbps over microwave links [8]) for the CSI to be available at the central unit. Hence, various joint processing schemes are developed to reduce the burden on backhauling. The *partial joint processing* algorithm is one such scheme, where only a subset of BSs are allowed to transmit based on a threshold. Thus, reducing the load on backhauling. Contrary to the centralized joint processing, the precoding can be done locally at each BS, which gives rise to *distributed joint processing*.

The performance gains involving multiple antennas over conventional techniques are tremendous. In the paper of Foschini [9], it was proved that the capacity increases with the minimum number of antennas over the transmitter

(Tx) and the receiver (Rx), without increasing bandwidth or power. Some of the benefits of MIMO are array gain, diversity gain, multiplexing gain, interference reduction and avoidance, but to exploit all of this may not be possible. Nevertheless, the performance gain in spectral efficiency due to the coordination of multiple antennas is shown in [3], i.e., there is a significant increase in spectral efficiency as the number of coordinated antennas is increased. However, without coordination, the increase in spectral efficiency is small with the increase in the number of antennas.

Coordinating multiple BS antennas in general is referred to as *Network MIMO* (NW MIMO), *Distributed Antenna Systems* (DAS) and *Joint Transmission* (JT).

1.2.1 Classification of Coordinated MultiPoint techniques

Coordination between BSs can be achieved on the Uplink (UL) and Downlink (DL). When there is coordination in the UL, this is referred as CoMP reception or Joint Detection. The received UL signal at multiple BSs may be combined using techniques such as Maximum Ratio Combining (MRC), etc. This is perceived to be implementation dependent with no impact on the radio interface. Coordination in the DL is referred to as Coordinated MultiPoint transmission or Joint Transmission. In MU-MIMO, the DL and the UL correspond to the Broadcast (BC) and Multiple Access Channel (MAC), respectively. The CoMP transmission can be compared to the MU-MIMO BC. In this thesis, the focus is on CoMP transmission and henceforth, any reference to CoMP refers to the DL transmission. As per [2] and [10], in the downlink the coordination multipoint schemes are divided into:

a) Dynamic scheduling achieved through coordination between multiple cells (is an extension of ICI coordination in LTE Release 8). 3GPP TR36.814 refers to this as *Coordinated Scheduling* or *Coordinated Beamforming* where the data to a Mobile Station (MS) is transmitted from one of the BSs and as the name suggests the scheduling decisions are coordinated. (See Figure 1.1 a). Due to this, only the generated beams and scheduling decisions need to be coordinated. The user data only needs to be present at one serving BS, unlike Joint transmission, discussed next.

b) Joint transmission and reception among multiple cells. 3GPP TR 36.814 refers to this as *Joint Processing/Transmission* where a single MS receives its data from various BSs. Thus, improving the received signal strength and canceling interference. (See Figure 1.1 b). Coherent joint processing puts tremendous requirements on backhaul, as the user data needs to be present at all the coordinating BSs.

The theoretical gains in terms of average and cell-edge users throughput with joint processing CoMP are substantially larger compared to coordinated beamforming [11]. In this thesis, we are more focused on Joint Processing Coordinated MultiPoint Transmission.

1.2.2 Obstacles

Some of the obstacles in realizing CoMP are discussed below.

- Noncausal CSI: DPC achieves capacity in MU-MIMO but due to the complexity involved, this is not practically feasible.

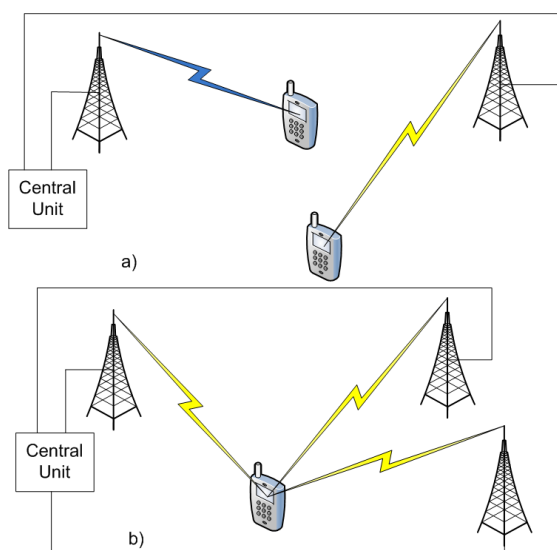


Figure 1.1: a) Coordinated Scheduling or Coordinated Beamforming b) Joint Processing / Transmission.

- Delay: The time delay in sharing information between BSs results in CSI mismatch, as the channel when measured for precoding is now different. Hence, with coherent joint processing, one needs to consider the trade-off between the latency involved in backhauling and the gains achievable with CoMP.
- Synchronization: The signals shared between BSs need to be time and phase synchronized. This tight synchronization puts tremendous requirements for high speed backhauling. The coordination algorithms implemented at the FPGA (Field Programmable Gate Array) level gives better synchronization [12].
- CSI Availability:
 - Time Division Duplex (TDD) can exploit the reciprocal nature of UL and DL such that the CSI estimated at the BS on the UL can in turn be used in the DL. Hence, no CSI feedback from the MS is necessary. This reciprocal nature holds good as long as the transmit frequency and the receive frequency are within the coherence bandwidth ($B_c \propto 1/T_D$, where B_c is the bandwidth over which the fading remains correlated and T_D is the delay spread) of the channel [13].
 - In case of Frequency Division Duplex (FDD), the UL and DL transmissions are on different frequencies. Hence, CSI feedback from MS is indeed necessary and various techniques exist in the literature.
- Impact of feedback errors: The potential errors due to quantization or data compression algorithms used by the MS to feedback the CSI will affect the beamformer.

The above obstacles tend to point that there will not be perfect CSI at the transmitter and then, imperfect CSI should be considered. However, in this thesis, perfect channel knowledge is assumed and imperfect CSI is part of the proposed future work. If the WINNER channel model is available with the time evolution feature being enabled, the delay in sharing information can be more realistically simulated.

1.3 Scope of this thesis

Three joint processing algorithms were earlier studied for a flat fading Rayleigh channel [14]. In this thesis, we extend this work, through the evaluation of the performance of these algorithms in a frequency selective channel using WINNER II channel model. An OFDM approach is used to exploit the frequency selective nature of the channel. In particular, these joint processing algorithms are applied in the frequency domain, in every subcarrier or a group of subcarriers, c.f., resource block (RB) in 3GPP LTE [15]. Considering the worst case scenario and maintaining fairness, all users are scheduled all the time in all the RBs.

The main focus is on the impact of the frequency selective channel on Partial Joint Processing (PJP) schemes. To form an active set in PJP, two different thresholding approaches are evaluated: the frequency adaptive thresholding and the non-adaptive frequency thresholding. As expected, the PJP schemes have higher average sum-rate per cell per RB with frequency adaptive thresholding compared to the non-adaptive thresholding.

Based on the numerical results, the PJP with a 5dB of threshold (in short written as PJP-5dB), the frequency adaptive thresholding improves the average sum-rate per cell per RB by $\sim 3\%$ for WINNER B1 (urban micro-cell) scenario, with respect to non-adaptive frequency thresholding. While an improvement of $\sim 25\%$ is observed in case of C1 (suburban macro-cell) scenario. This gain comes at the cost of an increased user data exchange. However, on an average less channel state information is fed back to the BSs. The reduced number of links give rise to limited CSI being available at the central unit for interference cancellation. Hence, a partial zero-forcing beamformer is used.

The rank deficiency of the scaled channel correlation matrices involved in the partial zero-forcing beamformer design arises for low values of active set threshold and for users closer to the BS. Hence, an algorithm is proposed that defines the cooperation area over the cluster where the PJP scheme with frequency adaptive or non-adaptive frequency thresholding can be applied and fall back on CJP or DJP schemes as needed. This algorithm dynamically chooses a joint processing scheme and hence this thesis is titled, "Dynamic Coordinated MultiPoint Transmission schemes".

1.4 Organization

This section presents how this document is organized. Chapter 2 sets the foundation for this thesis through the problem formulation. This chapter gives a detailed description of the system model which primarily consists of the joint processing algorithms being applied to the state of the art WINNER II channel

model. The generation of the channel matrix, antennas for the BS/MS and how they are laid out in a cellular environment are discussed under the section of WINNER II channel model. The joint processing algorithms such as the Centralized Joint Processing, Partial Joint Processing and Distributed Joint Processing algorithms are briefly discussed.

The simulation results with detailed discussions are presented in Chapter 3. Chapter 4 presents the conclusions derived from this thesis and highlights some of the future work under this WINNER/Joint Processing framework.

Finally, part of this work has been accepted for publication in the *IEEE 72nd Vehicular Technology Conference*. The paper is appended under a separate chapter titled Publication. Additional plots and intermediate results are presented in the appendix A for completeness. During this thesis, one of the goals was to reduce the overall execution time of this framework. Some of the MATLAB techniques used to speed up execution are discussed in appendix B.

Chapter 2

Problem Formulation

There Joint processing (JP) algorithms for CoMP transmission schemes were well studied for a flat fading Rayleigh channel [14]. The performance of these JP algorithms in a frequency selective channel is not known. The aim of this thesis is to extend the previous work [14] to a more realistic channel. To address this, one needs to develop a framework that can create a variety of realistic wireless channels based on various scenarios. The WINNER II Channel model offers a perfect platform for developing such scenarios, and the frequency selectivity of the wireless channel can be exploited using an Orthogonal Frequency Division Multiplexing (OFDM).

This chapter is the foundation of this thesis work.

2.1 System Model

Consider a hexagonal cell with a BS at its center with N_T antennas. This cell is divided into S sectors with frequency reuse factor of one. A set of K such BSs which intend to cooperate form a *cluster*. In this cluster, M mobile users with N_R antennas are served. It also follows that $N_T, K, N_R, M, S \in \mathbb{N}$. The set of BSs within the cluster can cause interference due to overloading or loss of orthogonality in any dimension, and the transmissions from BSs outside this set give rise to intercluster interference.

The JP algorithms considered are Centralized Joint Processing (CJP), where the central unit receives the CSI from all the BSs in the cluster for linear beamforming and power allocation. The Partial Joint Processing (PJP) scheme involves forming a subcluster of BSs such that the user receives the data from a subset of BSs. The Distributed Joint Processing (DJP) scheme performs beamforming and power allocation locally at each BS, based on local CSI information. The user can receive data from BSs other than the local serving BS. Section 2.3 presents a more detailed discussion on the JP algorithms.

Based on the technique used to form the clusters, they can be classified as either static or dynamic. A cooperating set of BSs which do not change with time is treated as static clustering, while dynamic clustering is a set of cooperating BSs which changes with time, i.e., BSs get added or removed from this cooperative set. In this thesis, we consider a static cluster of BSs w.r.t. CJP but in the case of PJP, the subset of BSs forms a dynamic subcluster for

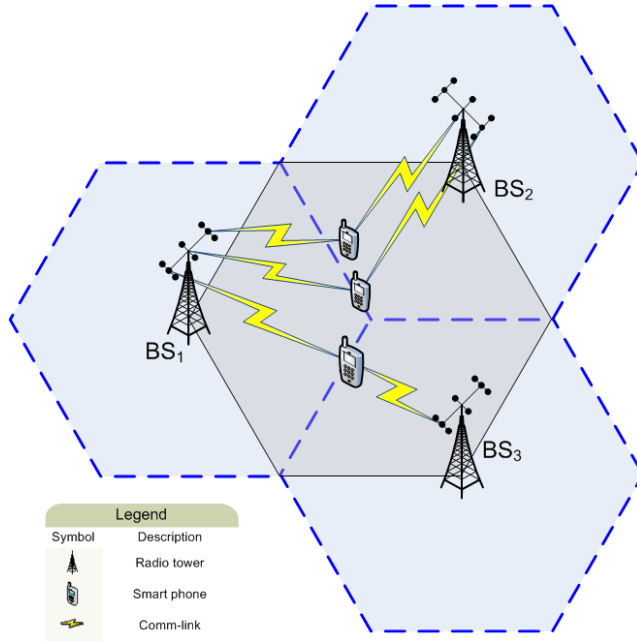


Figure 2.1: Layout: The gray hexagon in the middle is the cluster area. The dashed lines are the cell-edge regions.

each user in the cluster area. Depending on where the decision for JP is taken, (i.e., which set of BSs will be involved in JP) the clustering techniques can be divided into network-centric or user-centric. In the CJP scheme, the clustering is carried out at the network level, hence the CJP can be viewed as network-centric. While in the PJP scheme, the MS forms the subcluster of BSs, hence, PJP is a user-centric clustering technique.

In this thesis, we consider a static cluster with three BSs ($K = 3$) with three antennas ($N_T = 3$). Each BS serves three sectors ($S = 3$), i.e., 120° sectors and this set of BSs serve M single antenna users ($N_R = 1$) in the cluster area. The hexagon in the middle of Figure 2.1 shows such a cluster layout.

The cluster layout of BSs, mobile users, and the communication links are generated with the WINNER II Channel model for a given scenario. For example, the channel conditions in a Manhattan grid or an urban micro-cell can be generated and the JP algorithms can be applied. A complete discussion on the WINNER II channel model is described in section 2.2.

The frequency selectivity of the channel is exploited using OFDM. Considering the worst case scenario of an interference limited system and to maintain fairness in this system model, all the users are scheduled in every RB in the downlink (see section 2.4 for more details). The JP algorithms are applied in the frequency domain in every RB, to remove the interference between users. Hence, the discrete-time received signal, $\mathbf{y} \in \mathbb{C}^{M \times 1}$ at the M users can be expressed as

$$\mathbf{y} = \mathbf{H}\mathbf{W}\sqrt{\mathbf{P}}\mathbf{x} + \mathbf{n}, \quad (2.1)$$

where $\mathbf{H} \in \mathbb{C}^{M \times KN_T}$ is the channel matrix, $\mathbf{W} \in \mathbb{C}^{KN_T \times M}$ is the beamforming

matrix and $\mathbf{P} \in \mathbb{R}^{M \times M}$ is the power allocation matrix. The transmitted symbols $\mathbf{x} \in \mathbb{C}^{M \times 1}$ are normalized to unit power, and the receiver noise $\mathbf{n} \in \mathbb{R}^{M \times 1}$ with AWGN elements, each with variance σ^2 .

In equation (2.1), the channel matrix \mathbf{H} is of the form

$$\mathbf{H} = [\mathbf{h}_1^T \mathbf{h}_2^T \dots \mathbf{h}_M^T]^T, \quad (2.2)$$

where $\mathbf{h}_m \in \mathbb{C}^{1 \times KN_T}$ is the channel from the m th user to all the BSs in the cluster. The beamforming matrix \mathbf{W} is

$$\mathbf{W} = [\mathbf{w}_1 \mathbf{w}_2 \dots \mathbf{w}_M], \quad (2.3)$$

where $\mathbf{w}_m \in \mathbb{C}^{KN_T \times 1}$ is the beamformer for the m th user. Considering the individual \mathbf{h}_m being available from all the BSs at the central unit for joint processing (CJP), the multiuser interference with a zero-forcing beamforming design, taking the pseudoinverse of \mathbf{H} ,

$$\mathbf{W} = \mathbf{H}^H (\mathbf{H}\mathbf{H}^H)^{-1}. \quad (2.4)$$

The intracluster interference is completely removed, i.e., $\mathbf{H}\mathbf{W} = \mathbf{I}$, where $\mathbf{I} \in \mathbb{R}^{M \times M}$ is an identity matrix, when $KN_T \geq M$ for the entire cluster [16]. At every BS, the maximum power is restricted to P_{max} . Then, the power allocation matrix based on [7] becomes

$$\mathbf{P} = \left\{ \min_{k=1, \dots, K} \left(\frac{P_{max}}{\|\mathbf{W}^k\|_F^2} \right) \right\} \cdot \mathbf{I}_M, \quad (2.5)$$

where \mathbf{W}^k are the rows of the matrix \mathbf{W} related to the k th BS. This power allocation is suboptimal, since it typically results in only one of the BSs meeting the maximum transmitted power requirement with equality, and hence, the remaining BSs transmit below the P_{max} value.

This model can be generalized to multiple cluster scenario. Hence, at the OFDM sub-carrier level, equation (2.1) for a particular i th cluster becomes,

$$\mathbf{y}_i = \mathbf{H}_i \mathbf{W}_i \sqrt{\mathbf{P}_i} \mathbf{x}_i + \mathbf{n}. \quad (2.6)$$

The received downlink signal for the m th user in the i th cluster, considering all the clusters is

$$y_{i,m} = \underbrace{\mathbf{h}_{i,m} \mathbf{w}_{i,m} \sqrt{p_{i,m}} x_{i,m}}_{\text{Desired Signal}} + \underbrace{\sum_{\substack{j=1 \\ j \neq m}}^M \mathbf{h}_{i,m} \mathbf{w}_{i,j} \sqrt{p_{i,j}} x_{i,j}}_{\text{Intracluster Interference}} + \underbrace{\sum_{\forall i' \neq i} \sum_{j=1}^M \mathbf{h}_{i',m} \mathbf{w}_{i',j} \sqrt{p_{i',j}} x_{i',j}}_{\text{Intercluster Interference}} + n, \quad (2.7)$$

where $\mathbf{h}_{i,m}$, $\mathbf{w}_{i,m}$ and $\sqrt{p_{i,m}}$ are the channel, the beamformer and the power at which the signal is transmitted to the m th user in the i th cluster, respectively. This forms part of the desired signal. The $\mathbf{w}_{i,j}$ and $\sqrt{p_{i,j}}$ is the beamformer and the power allocated to the j th user in the i th cluster, respectively. This affects the desired signal within the same cluster due to the transmission to

users other than the m th user. Hence, this forms the Intracluster interference. The i ' corresponds to the transmission to users in all the clusters. The interference generated in clusters other than the i th cluster forms the intercluster interference.

If the receiver can intelligently combine its received signals using for example, MRC or selection combining or threshold combining with weights \mathbf{r}_m , then the Signal to Interference plus Noise Ratio (SINR) at the m th user in the i th cluster is

$$\text{SINR}_{i,m} = \frac{\|\mathbf{r}_m^H \mathbf{h}_{i,m} \mathbf{w}_{i,m}\|^2 p_{i,m}}{\sum_{\substack{j=1 \\ j \neq m}}^M \|\mathbf{r}_m^H \mathbf{h}_{i,m} \mathbf{w}_{i,j}\|^2 p_{i,j} + \sum_{\forall i' \neq i, j=1}^M \|\mathbf{r}_m^H \mathbf{h}_{i',m} \mathbf{w}_{i',j}\|^2 p_{i',j} + \sigma^2} \quad (2.8)$$

For simplicity, in this thesis, the intercluster interference is assumed to be perfectly removed and the receiver combining weights are not considered. Hence, the generalized SINR in the above equation (2.8) simplifies to

$$\text{SINR}_{i,m} = \frac{\|\mathbf{h}_{i,m} \mathbf{w}_{i,m}\|^2 p_{i,m}}{\sum_{\substack{j=1 \\ j \neq m}}^M \|\mathbf{h}_{i,m} \mathbf{w}_{i,j}\|^2 p_{i,j} + \sigma^2} \quad (2.9)$$

Assuming coherent reception, the average sum-rate per cell achieved in the cluster area for a given RB is

$$SR_{RB} = \frac{1}{K} \mathbb{E}_H \left\{ \sum_{m=1}^M \log_2 (1 + \text{SINR}_{i,m}) \right\} [\text{bits/s/Hz/cell}] \quad (2.10)$$

This can also be referred to as spectrum efficiency. ITU-R [17] specifies the expected sum-rate at layer 3 but here we are dealing at the actual physical layer without pilots.

2.2 WINNER II Channel Model

The WINNER project was developed by a consortium of companies and universities, to develop a single ubiquitous radio system. The WINNER II Channel Model (WIM2) currently represents the state of the art in wireless channel modeling. The WINNER channel models are antenna independent, i.e., different antenna element patterns can be introduced. It also made provisions to construct a 3-D Antenna Array [18] and to specify the number of antennas for the MSs or BSs. Once the MSs and the BSs are built, then their location can be specified with mobility. The layout of a cellular system can be constructed, with these stations placed as needed. The height of the stations can also be specified or taken from a given WINNER scenario. The scenarios (B1, C1, etc) are based on both extensive real life measurement campaigns and literature. The propagation conditions of the channel can be generated based on the scenario, antenna arrays and the location of stations. The scenarios having a Line of Sight (LOS) or Non-Line of Sight (NLOS) are derived from a probability distribution. In

the WIM2 context, a cluster consists of a number of rays, it is the propagation path diffused in space. (Note: In this section of WIM2, the reference to cluster should not be confused with the cluster definition in CoMP). Hence, the MIMO channel matrix is given by

$$\mathbf{H}(\tau; t) = \sum_{n=1}^N \mathbf{H}_n(\tau; t), \quad (2.11)$$

where N is the number of paths and

$$\mathbf{H}_n(\tau; t) = \iint \mathbf{F}_{RX}(\varphi) \mathbf{h}_n(\tau; t, \phi, \varphi) \mathbf{F}_{TX}^T(\phi) d\phi d\varphi, \quad (2.12)$$

where the \mathbf{F}_{RX} and \mathbf{F}_{TX} are the antenna array response matrices, and \mathbf{h}_n is the channel response matrix for the n th cluster. In WIM2, a feature called the *intracluster delay spread* exists, where the two dominant clusters are divided into two subclusters each. The channel coefficients generated is a 4-D array consisting of number of antennas between the stations, the number of taps for a given scenario and the number of time samples. The WINNER II channel occupies a bandwidth of 100MHz. (Refer to [19] for more details). For comprehensive MATLAB details for creating antenna arrays, layout setup and channel generation, refer to [20].

2.2.1 Antenna Patterns

Dipole antennas with down-tilt of 12 degrees are used at the BS and an isotropic antenna is used at the MS. The individual antenna elements at the BS are positioned based on an element-coordinate-system (ECS) along its x-axis, as used in the default WIM2 configuration. They are placed 4λ apart which corresponds to 0.6m. This spacing was derived from [21]. The Uniform Linear Array (ULA) can be rotated with respect to the array-coordinate-system (ACS). The entire ULA can also be rotated in the global-coordinate-system (GCS) wherein the entire BS is moved. Refer to [18] and [20] for more details. The ULA at every BS is oriented towards the cluster-center based on GCS. 3GPP TR 25.996 [22] gives the BS antenna pattern and bore-sight configuration for 3 or 6 sectors cells for MIMO simulations but these were not used, as the CoMP related antenna patterns and bore-sight configurations are yet to be finalized. One of the intentions was to have similar configuration as that of EASY-C [23], hence, cross-polarized antennas were used at the terminals. This has no impact, as channel gains alone are calculated by the MS in the JP schemes. The radiation patterns of a single antenna at the BS and MS are shown in Figure 2.2. The original radiation pattern is a thick blue line and based on [18], a 2D Fourier Transform is used to store the beam pattern efficiently as the Effective Aperture Distribution Function (EADF). Based on the plot generated, this EADF overlaps the original pattern. The total radiation pattern is shown in appendix A.1.

2.2.2 The Grid Layout

The performance of the CJP, PJP and DJP schemes is evaluated over the cluster area. Hence, the cluster area previously defined in Figure 2.1 is divided into $54 + 3$ positions, as shown in the Figure 2.3. The Cartesian coordinate system

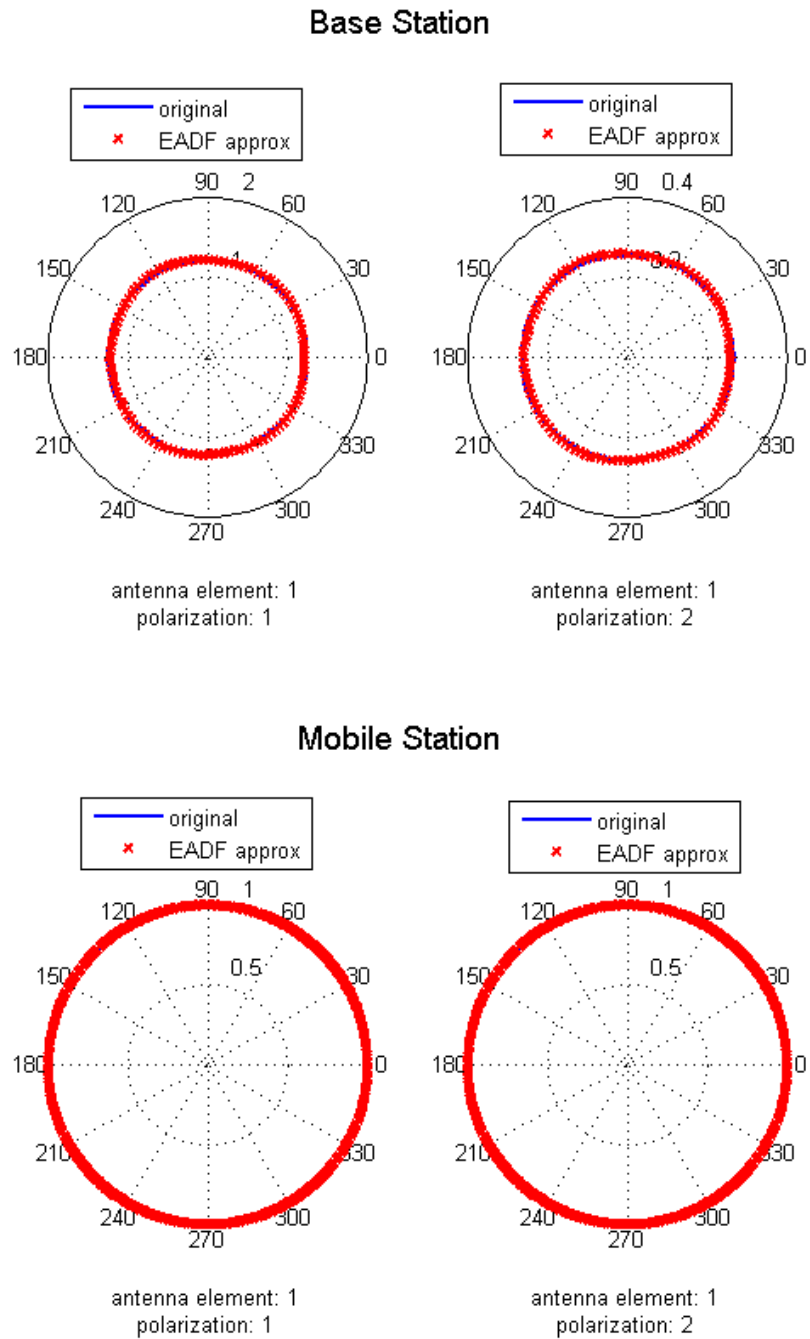


Figure 2.2: Radiation Pattern of the Antenna 1 of BS and the MS (Generated using WIM2).

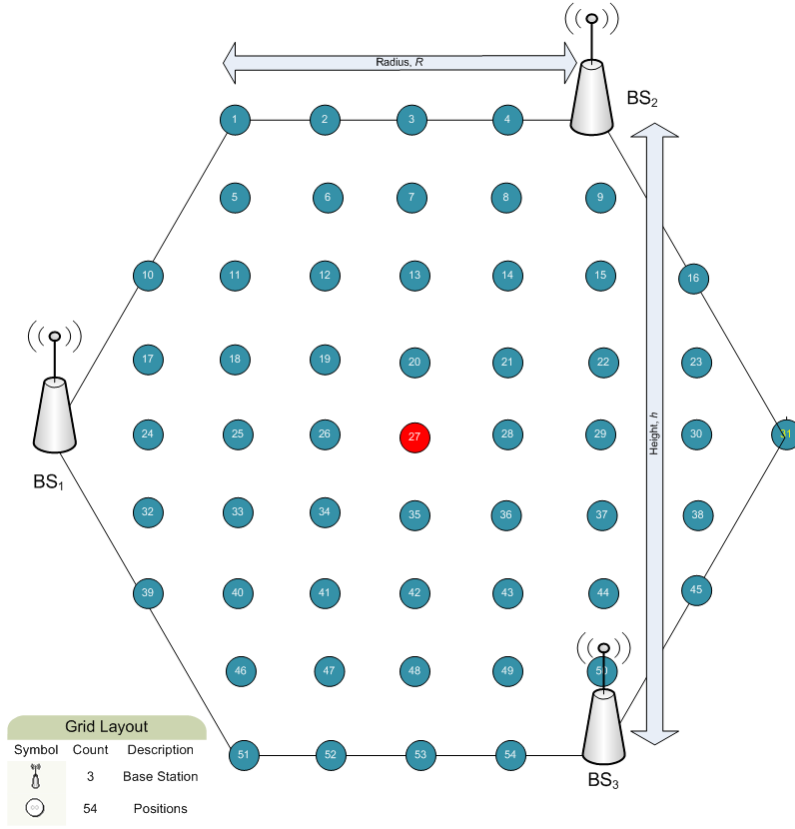


Figure 2.3: Grid of positions over the cluster area. Position 27 corresponds to the cluster-center.

is overlaid on the hexagonal cluster area, such that the origin is located at the center of the hexagon. The origin is also called the cluster-center. The hexagon with various positions forms a grid. This is the grid layout considered in [14]. The three BSs have a cell radius of $R = 500m$ and are placed on the alternate vertices of this regular hexagon. The distance between any 2 BSs is the height of the hexagon ($h = \sqrt{3} \cdot R$).

The MSs are dropped at a particular position on the grid layout, $(x \pm \Delta x, y \pm \Delta y)$, where (x, y) is the position on the grid and $\Delta x \leq \frac{R}{16}$ and $\Delta y \leq \frac{h/2}{16}$ [14]. R is the radius of the cell and h is the height of the regular hexagon. (See Figure 2.3). The users are uniformly dropped along an ellipse with $\pm \Delta x$ and $\pm \Delta y$ forming the major axis and the minor axis, respectively.

2.2.3 Channel Generation

Moving users are dropped at specific locations with an offset of $(\Delta x, \Delta y)$ over a position of the grid layout. The velocity of the user can be pictured as a vector in space, where its magnitude can be seen as the speed of the user and its angle is the direction in which the user is traveling. This speed is fixed at 3 km/h while the direction is randomly generated. Figure 2.4 shows three users dropped

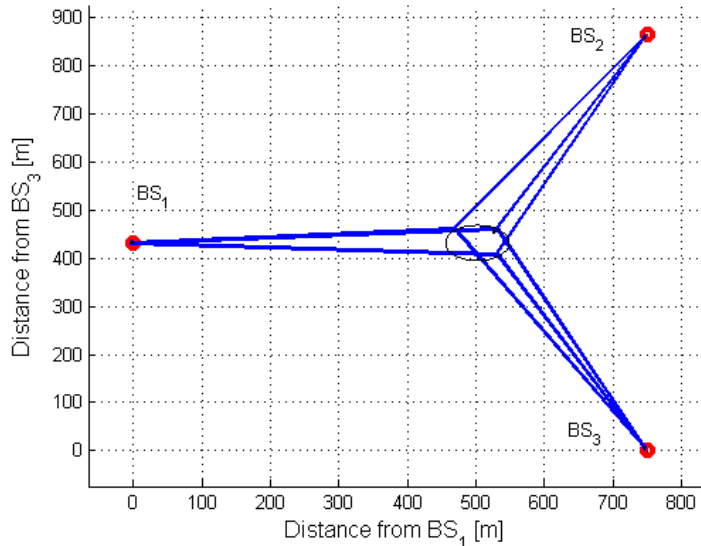


Figure 2.4: Layout: At the cluster-center (Position 27), 3 users are dropped along an ellipse. The red circles denote the BSs (Generated using WIM2).

at the cluster-center. The users are linked with all the three BSs.

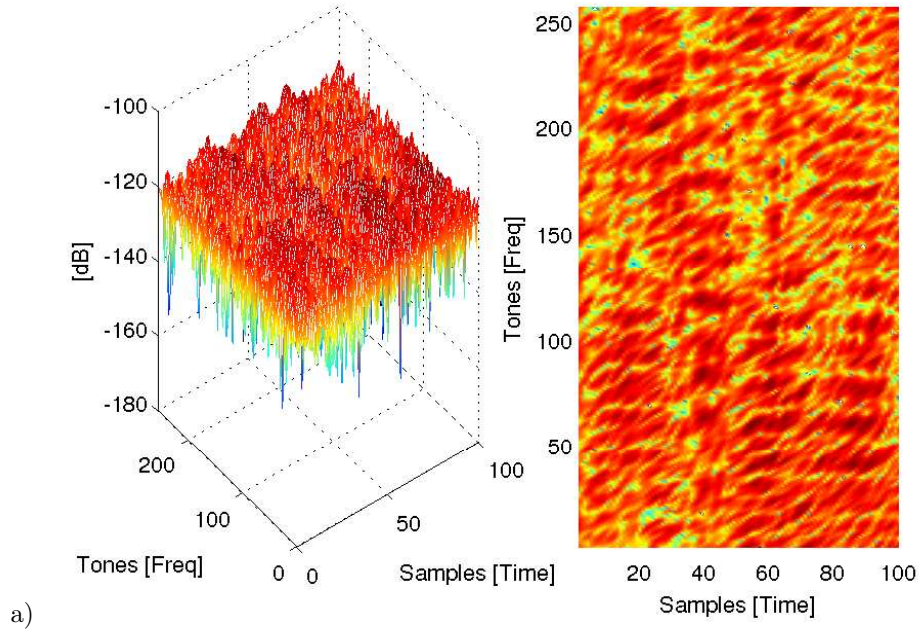
When the users are dropped, the channel seen by the user is a snapshot of the propagation environment. In a channel segment, the user velocity and shadow fading parameters are considered constant. According to WINNER [19], a drop is defined when the channel segment goes to zero. When this happens, the motion of the user is considered virtual, due to which there is fast fading and the superposition of rays gives rise to Doppler while all other parameters are fixed. Such consecutive drops are uncorrelated. The channels observed by one of the users with respect to one of the BS antennas are shown in Figure 2.5 for various WINNER scenarios. In these figures, along the time axis, every channel segment or time sample is uncorrelated, as each one of them is formed due to a drop. Every time samples represented in these figures are uncorrelated. The WINNER II channel model has a unique feature of time evolution, where the consecutive time samples are correlated which gives a sense of how the channel has evolved over time. Presently, this feature is disabled in the WINNER MATLAB code. (Refer [19] for more details). For the simulations, we only consider a single time sample for every drop (in every channel realization).

WIM2 is modified such that all users receive the transmission from all the BSs. The links generated are completely NLOS. The pathloss and shadow fading are multiplied with the channel matrix.

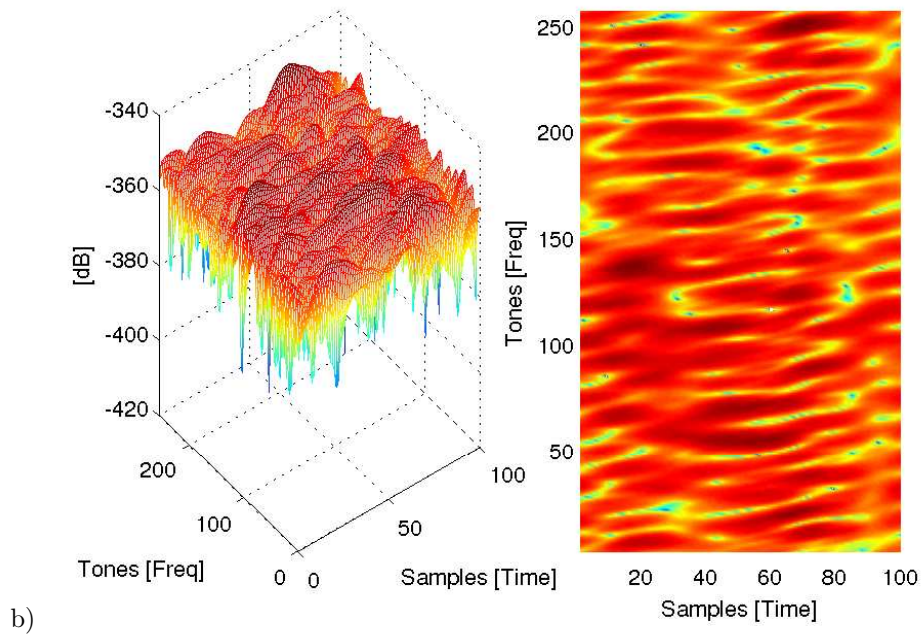
2.3 Joint Processing Algorithms

With the increase in the numbers of users, there is a proportional increase in the feedback of CSI to the BSs. This poses very high backhauling requirements for the BSs to cooperate. Thus, suitable JP algorithms are needed to reduce

B1-Urban micro-cell



A2-Indoor to Outdoor



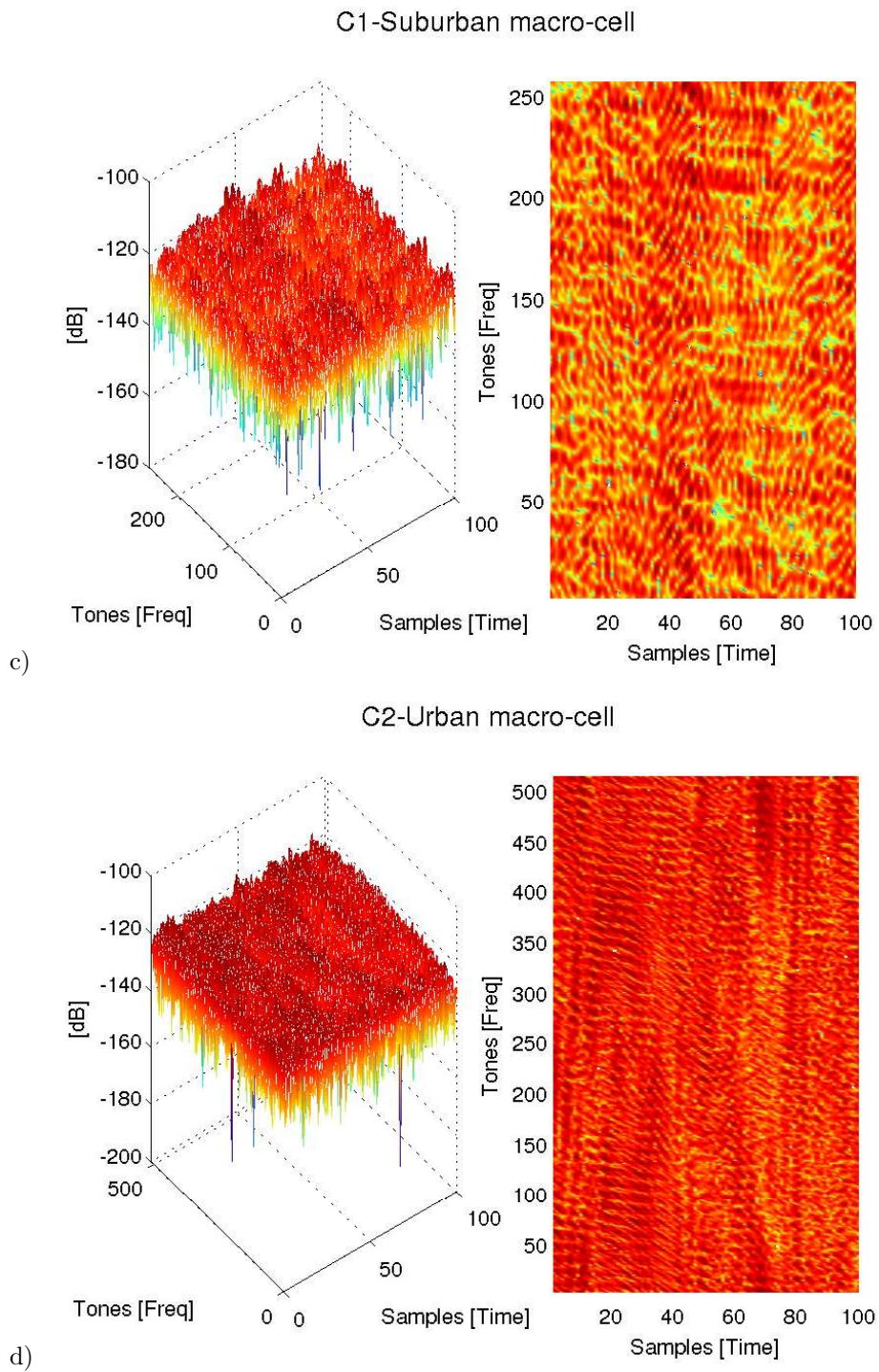


Figure 2.5: A typical NLOS channel from one of the antennas of the BS to the mobile user at the cluster-center for a) B1-Urban micro-cell b) A2-Indoor to Outdoor c) C1-Suburban macro-cell and d) C2-Urban macro-cell.

this burden on the backhaul.

2.3.1 Centralized Joint Processing (CJP)

The user needs to feedback the CSI from all the BSs in the cluster to the serving BS. This information is passed onto a central unit for interference avoidance. The central unit is an additional component in the network or it can reside in one of the BSs of the cluster. The central unit uses this global CSI for power allocation and beamforming. In this approach, given that the beamformer is well conditioned and the central unit has the complete CSI, the intracluster interference is completely removed. This algorithm poses tremendous requirements on backhauling, since the CSI from all the cooperating BSs needs to be available at the central unit for precoding.

2.3.2 Distributed Joint Processing (DJP)

In the Distributed Joint Processing (DJP), as the name suggests, the power allocation and beamforming are calculated at each BS, locally. In this approach, JP is still allowed as the users can receive data from other BSs. A multibase scheduling algorithm is required to schedule the users. As the number of users served is limited by the number of antennas at each BS. In the spatial domain, this gives rise to some users in outage [24].

2.3.3 Partial Joint Processing (PJP)

The PJP algorithm is a threshold based window approach, where those BSs within the cluster whose links with the user fall within this window are included in the active set of the user and are allowed to cooperate. This window is a threshold level that is given by the cluster to the user. The user takes its best channel as its reference or serving BS link and sorts the links with the remaining BSs in the cluster relative to this reference link. This ordering is based on the channel strength or energy of the frequency selective channel, $\mathbf{h}_{i,m}(\tau; t)$ for the m th user, where τ is the tap delay in that time instant t . The PJP algorithm is a particular case of CJP and it asymptotically reaches the CJP performance when the active set threshold goes to infinity. Those BS links which fall within this given threshold are made active and those that fall outside this threshold are marked inactive. These active and inactive links are represented by ‘1’ and ‘0’, respectively, forming a *non-adaptive frequency* thresholding matrix, $\mathbf{T}^{NA} \in \{0, 1\}$ of size $[M \times K]$. Notice that $\mathbf{T}_{(m,k)}^{NA} = 1$ means that the link between the BS k in the cluster and the user m is active. In the non-adaptive frequency case, the active set thresholding is performed over an average of all the RBs. This active set of BSs is used in all the RBs but the user needs to feed back the CSI of these active links per RB.

With a realistic wideband channel, one can exploit the frequency selectivity by performing the active set thresholding in every RB. This adaptive thresholding approach is called *frequency adaptive* thresholding. The frequency adaptive thresholding approach defines a \mathbf{T}^{FA} matrix in each RB. As a drawback, the active set of BSs may change in each RB. The backhauling load is increased, since the user data needs to be available in all the BSs of the cluster.

As we later show in the simulation results, frequency adaptive thresholding does improve the average sum-rate per cell per RB compared to the non-adaptive frequency thresholding, but at the cost of an increased user data exchange over the backhaul. With the PJP scheme, there is very limited CSI available for designing the beamformer, specially when the user is close to the BS and the active set threshold value is low. This motivates us to develop a partial zero-forcing beamformer based on the proposal in [25].

2.4 Resource Block Allocation

Consider a multipath channel $\mathbf{H}(\tau; t)$ where τ is the tap delays of the channel and t is the time instant. Taking the Discrete Fourier Transform (DFT), we get

$$\mathbf{H}(\tau; t) \xrightarrow{\frac{\mathcal{F}_\tau}{N}} \mathbf{H}(f; t). \quad (2.13)$$

A Fast Fourier Transform (FFT) is used to realize the DFT. Depending on the WINNER scenarios, the longest tap delay defines the FFT size, N , and is typically rounded to the next power of 2. N is chosen to be sufficiently large such that the bandwidth of the channel is lesser than the coherence bandwidth of the channel, so that the OFDM subcarriers observe a flat fading channel. Every user at a given position on the grid sees the signal from all the BSs across all the antennas. Hence, the channel matrix for the m th user in the a th subcarrier is $\mathbf{h}_m(f_a; t)$ of size $1 \times KN_T$. For simplicity, we will assume one subcarrier per RB. To consider the worst case interference scenario, all users are scheduled in all the RBs. Hence, the a th subcarrier of every user will be scheduled in the a th RB. The JP algorithms can be applied in every RB, i.e., the ZFBF does interference avoidance in the frequency domain in every RB.

The Figure 2.6 a) shows a typical multipath channel matrix. Here WINNER scenario B1 is considered, which has 20 clusters (multipaths). At a given time instant T_0 , user-1 sees the links from all the BSs. Since each BS has 3 antennas, they are represented with 3 columns. The tap delays between user-1 and BS-1 is given by H11 and likewise with other BSs. On taking the 256-point FFT we get Figure 2.6 b), where every row represents a subcarrier. The colors are only highlighted to show how the RB is formed in Figure 2.6 c). Considering only 3 users, this figure also shows that all users are scheduled in a RB and JP is applied in this RB of the same frequency to remove the interference for the downlink transmission to the users. As there are 256 subcarriers, we have 256 RBs. The complete structure of the entire RB is shown in Figure 2.7.

2.5 Partial Zero-Forcing Beamforming

The partial zero-forcing beamformer is derived in this section for both frequency adaptive and non-adaptive frequency thresholding approaches. The partial zero-forcing technique proposed in [25] is based on the definition of a useful matrix and interference matrices that modify the channel matrix to obtain useful and interference channel matrices. In our case, \mathbf{T}^{NA} and \mathbf{T}^{FA} active link matrices are the basis for defining them. For a given time instant t , and considering the a th RB of the M users in the i th cluster (All calculations are performed in the

2.5. PARTIAL ZERO-FORCING BEAMFORMING

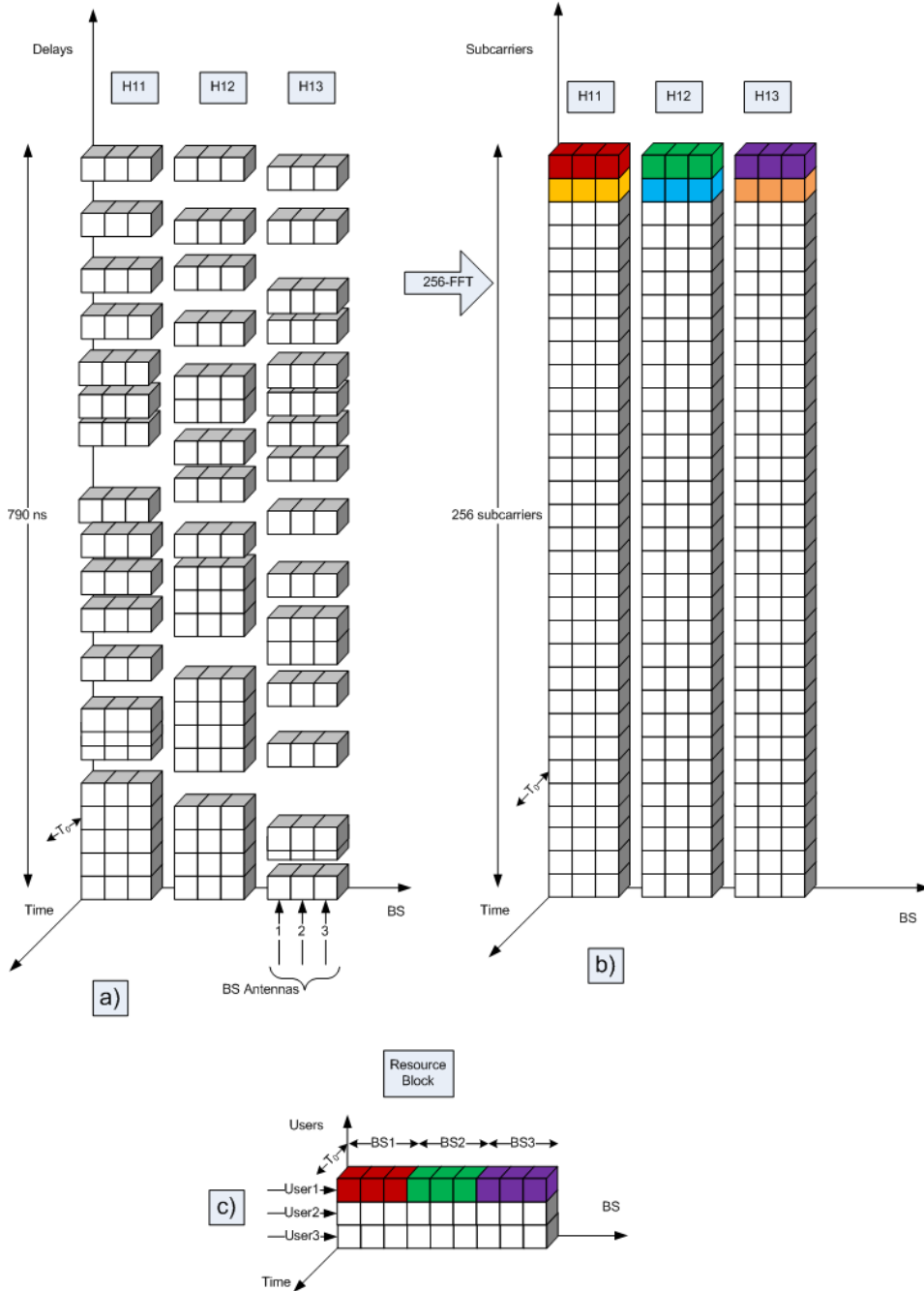


Figure 2.6: a) $\mathbf{H}(\tau; t)$ for a WINNER B1 NLOS scenario b) $\mathbf{H}(f; t)$ after a 256-point FFT c) Resource block for a given subcarrier.

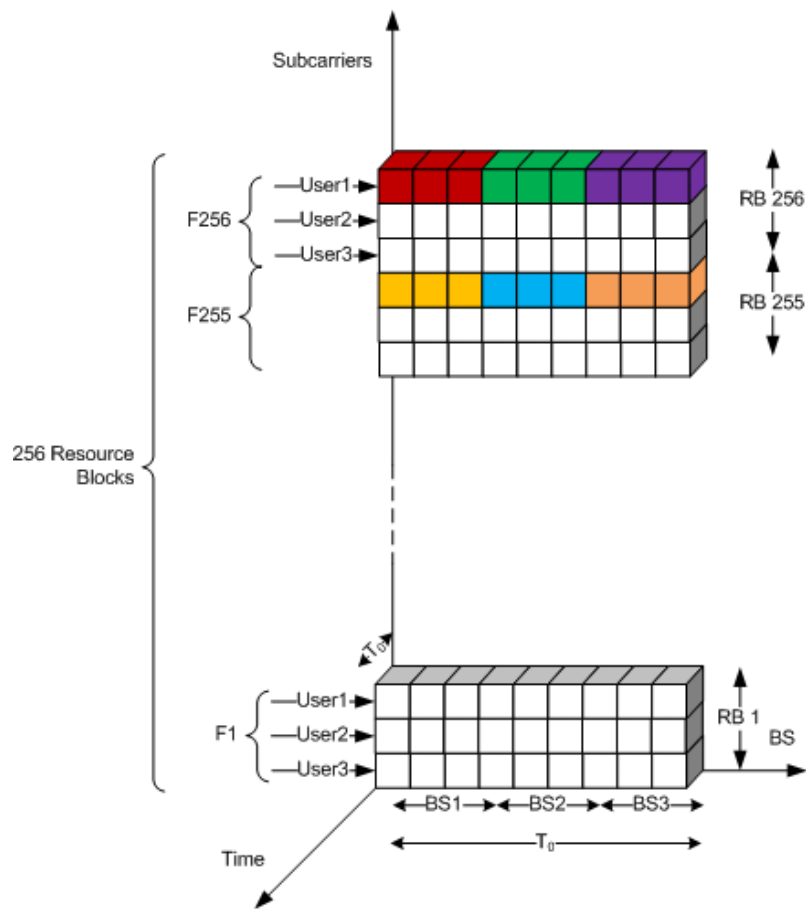


Figure 2.7: The complete Resource Block structure.

i th cluster and for notational convenience the suffix i is dropped), the useful channel matrix $\mathbf{U}_x \in \mathbb{C}^{M \times KN_T}$ is defined as

$$\mathbf{U}_x = [\mathbf{T}^x \otimes \mathbf{1}_{N_T}] \odot \mathbf{H}(f_a; t), \quad (2.14)$$

where \otimes is the Kronecker product, $\mathbf{1}_{N_T}$ is an all ones N_T row vector and \odot is the element-wise multiplication operation. x represents either TA or NA and f_a is the center frequency of the a th RB.

Using the active link matrices \mathbf{T}^{NA} and \mathbf{T}^{FA} , one can construct the matrices of the interference caused due to the transmission to the m th user in the cluster, $\mathbf{T}_{m,Int}^{NA}$ and $\mathbf{T}_{m,Int}^{FA}$, respectively. The rules for building the interference matrices for the m th user are that the data destined to the user only affects those users that share the transmitting BS. Such links that cause interference are marked '1'. Conversely, the inactive links for this user obviously do not cause interference to other users and also, the active links do not cause interference to itself. Hence, such links are marked '0'. The interference matrices try to remove the interference generated due to the transmission to a user by explicitly forcing this interference to zero. Therefore, the interference channel matrix $\mathbf{V}_{x,m} \in \mathbb{C}^{M \times KN_T}$ introduced by the transmission to the m th user in the i th cluster in the a th RB can be written as

$$\mathbf{V}_{x,m} = [\mathbf{T}_{m,Int}^x \otimes \mathbf{1}_{N_T}] \odot \mathbf{H}(f_a; t). \quad (2.15)$$

Assuming that the iterative partial zero-forcing algorithm proposed in [25] converges, the partial zero-forcing beamformer $\mathbf{W}^x \in \mathbb{C}^{KN_T \times M}$ is given by

$$\mathbf{W}^x = \mathbf{U}_x^H \cdot (\mathbf{G}_x + \overline{diag}(\mathbf{R}_x))^{-1}, \quad (2.16)$$

where $\overline{diag}(\cdot)$ are the off-diagonal elements of the matrix. The matrix $\mathbf{G}_x \in \mathbb{R}^{M \times M}$ is the channel energy scaling matrix given as

$$\mathbf{G}_x = diag(\mathbf{U}_x \mathbf{U}_x^H) \cdot \mathbf{I}_M, \quad (2.17)$$

where $diag(\cdot)$ are the diagonal elements of the matrix. The channel correlation matrix $\mathbf{R}_x \in \mathbb{C}^{M \times M}$ is given as

$$\mathbf{R}_x = \left(\mathbf{V}_{x,1} \mathbf{U}_{x(1,:)}^H \cdots \mathbf{V}_{x,M} \mathbf{U}_{x(M,:)}^H \right). \quad (2.18)$$

The partial zero-forcing beamformer can only be used when the scaled channel correlation matrix

$$\mathbf{Q}_x = [\mathbf{G}_x + \overline{diag}(\mathbf{R}_x)], \quad (2.19)$$

is invertible. As we show in the simulation results in section 3.6, this condition is not always fulfilled, specially for low values of the active set threshold and users located close to a BS. Hence, we propose an Algorithm 3.1 to define a *cooperation area* for a given active set threshold value such that the frequency adaptive or non-adaptive PJP schemes can be performed.

Chapter 3

Simulation Results and Discussion

Prior to the start of this work, three JP algorithms were evaluated in [14] for a flat fading Rayleigh channel. In this thesis, we evaluate these JP algorithms for a frequency selective channel. An OFDM approach where these algorithms are applied in every RB, as all the users are served in every RB.

3.1 System Parameters

The system parameters are chosen based on the previous work [14] and enhanced based on the WINNER II channel model [20]. The 3GPP TR 25.996 Spatial Channel Model (SCM) for MIMO [22] specifies an antenna model but the verification of this configuration was not successful. Hence, an ULA of dipole antennas were used. The users are dropped at every position on the grid layout as explained in section 2.2.2 over 500 channel realizations. The complete system parameters are summarized in table 3.1.

3.2 Power allocation

The maximum power at which the BS can transmit is fixed at a P_{max} value. Per-BS power constraints is a more realistic assumption compared to a pooled or sum-power constraint, where the available power P_{max} is shared among the set of cooperating BSs (see [7]) and also practically due to amplifier constraints in the BSs. In the simulations, the P_{max} value is obtained for cell-edge SNR values (reference value for one user located at the cell-edge) ranging from 0 to 15 dB. This maximum power P_{max} is equally divided in all the RBs. See section 2.4 on how the users are allocated to the RBs, and the application of JP algorithms in these RBs. The power allocation matrix in equation (2.5) based on [7] says that only the BS satisfying the minimum value can transmit at full power and other BSs transmit with power less than P_{max} .

Table 3.1: Summary of System Parameters

Parameters	Values
Number of BSs, K	3
Sectors in each BS, S	3
Number of Users, M	3, 6, 9, 12
Number of Antennas at each BS, N_T	3
Number of Antennas at the each user, N_R	1
Type of Antenna	Dipole
Antenna types	Uniform Linear Array
Antenna spacing	$4\lambda^*$
BS Antenna down-tilt angle	12°
Number of positions on the grid	54
Number of channel realizations at each position	500
Frequency Reuse Factor	1
Center frequency	2 GHz
Channel Bandwidth	100 MHz
Operating Temperature	290 K
Signal to Noise Ratio, SNR	15 dB
Cell Radius, R	500 m
Cluster height or Inter-BS distance, h	$\sqrt{3}R = 433$ m
User speed	3 km/h
WINNER II Channel Model	B1, C1 and C2 **

* Based on a reference configuration used in *EASY-C* [21]

** All the results shown are based on NLOS channels unless other explicitly stated

3.3 Active Set Threshold value for various WINNER scenarios

In PJP, one of the main parameters is the active set threshold value. (See section 2.3.3 for more details). In Figure 3.1, it can be observed that the average number of BSs transmitting to a user, which depends on the *active set* (AS), highly changes depending on the simulated WINNER scenario. For example, for an AS threshold of 40dB, most of the WINNER scenarios have nearly all the BSs serving a user, but scenario A2 (Indoor-Outdoor) and B4 (Outdoor-Indoor), require a threshold greater than 100dB for all the 3 BSs to serve a user. Hence, when setting an AS threshold value for the PJP scheme, the scenario or channel conditions should also be considered. Furthermore, the central unit may even switch to another JP scheme such as the CJP or DJP if the system requirements are not fulfilled for any value of the PJP AS threshold.

In Figure 3.1, scenarios B1 (urban micro-cell), B2 (bad urban micro-cell) and C2 (urban macro-cell) possess rich scatters, hence they closely follow the flat fading Rayleigh curve. The scenario C1 (suburban macro-cell) shows a dip in the curve for AS thresholds around 20dB to 40dB, due to the fact that there is a dominant LOS in C1 which affects the pathloss. Scenarios A2 and B4 are completely NLOS with poor channel conditions. This forms an interesting case for selection of the threshold value. In general, the LOS probabilities are based

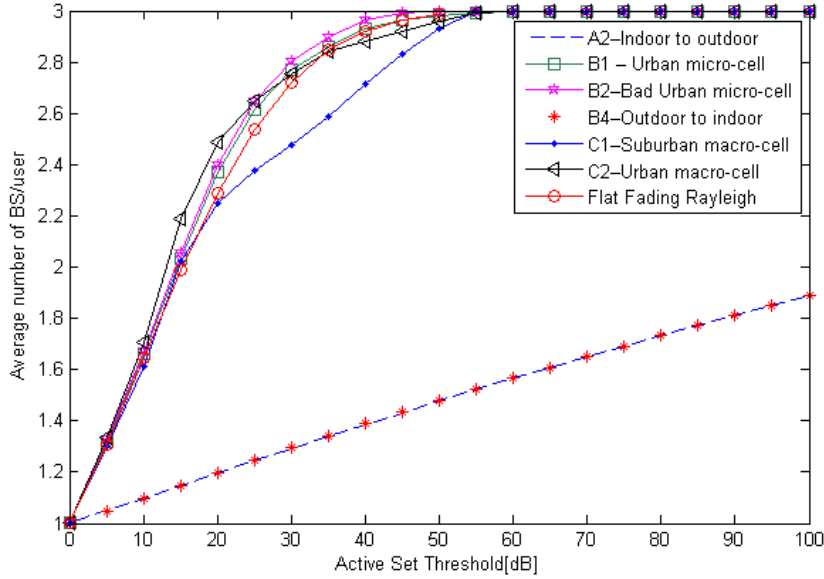


Figure 3.1: Average number of BS transmitting to a user for various WINNER scenarios (LOS & NLOS) when only pathloss and shadowing are considered.

on distance for a given scenario, refer Table 4-7 of [19].

The small scale fading effects are averaged out due to a Monte-Carlo type simulation, hence, in Figure 3.1, only pathloss and shadow fading are explicitly considered. A more detailed discussion of the impact of the WINNER channel scenario on the average number of BSs transmitted to a user is presented in appendix A.2.

3.4 The Sum-Rate

In the previous work [14], the average sum-rate of the JP algorithms was calculated for a flat fading Rayleigh channel over the entire grid area. This plot is shown in Figure 3.2 (reproduced with permission from the author [14]). In that work, the average sum-rate per cell for the different JP schemes is plotted from BS towards the cell-edge (see Figure 2.3).

Figure 3.3 shows the average sum-rate per cell per RB for the WINNER scenario B1 (NLOS) when non-adaptive frequency thresholding is considered in the PJP scheme. The JP schemes follow a similar order as in Figure 3.2. The CJP achieves the highest sum-rate at the cost of requiring complete CSI. The PJP scheme shows a decreasing effect on sum-rate with decreasing values of threshold due to reduced feedback and backhauling. Finally, the DJP scheme shows the lowest sum-rate, but only local CSI is needed.

The flat nature of curves in Figure 3.2 is not seen, instead, Figure 3.3 shows a more bell-shaped. One reason could be the gain attributed to using dipole antennas, which are separated by 4λ at the BS. Moreover, looking at the slope of the PJP curves along the normalized distance from BS₁, it appears that the

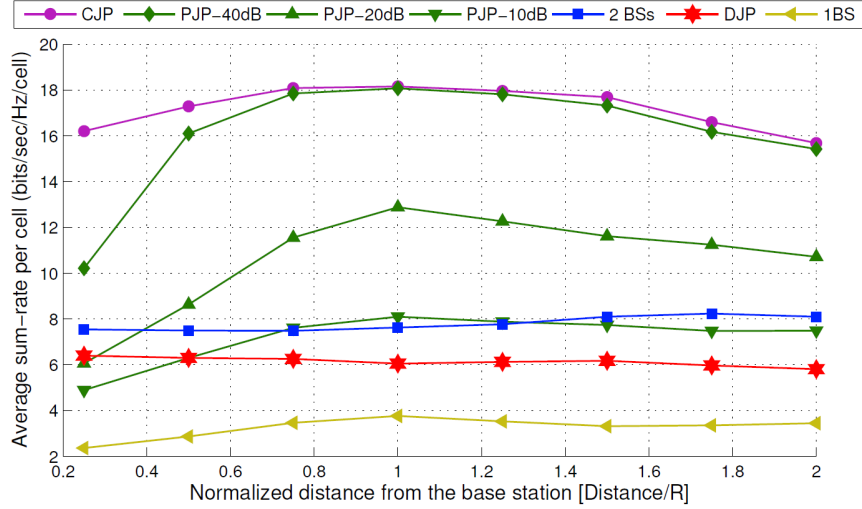


Figure 3.2: Prior work: Average sum-rate per cell along the normalized distance from BS_1 .

average sum-rate from BS_1 to the cluster-center is lesser than the average sum-rate from the cluster-center ($[Dist/R] = 1$) to the cell-edge ($[Dist/R]$ range from 1.2 to 2). Thus, JP does improve sum-rate especially for the cell-edge users. The cluster-center seems to have the highest average sum-rate and one of the main reason is that the cluster-center is the only location on the grid where all links from the BSs have a good opportunity for JP.

When frequency adaptive thresholding is considered in the PJP scheme, a similar bell-shaped plot is obtained but with improved average sum-rate. A better metric to compare both the non-adaptive frequency thresholding and frequency adaptive thresholding for the PJP scheme is the percentage gain in average sum-rate per RB with frequency adaptive thresholding (SR^{FA}) compared with non-adaptive frequency thresholding (SR^{NA}), given as

$$G_{SR}[\%] = \frac{SR^{FA} - SR^{NA}}{SR^{NA}}. \quad (3.1)$$

This is plotted in Figure 3.4 and 3.5 for WINNER scenarios B1 and C1, respectively. From these plots, we see that the DJP has the best gain, but we are interested in the analysis of the PJP. It is interesting to see that the PJP-5dB with frequency adaptive thresholding has very little gain in the B1 scenario and even negative gain in the C1 scenario at the cluster-center. This is possibly due to the thresholding window being too small, there is a high likelihood of having very few active links.

The results of various other WINNER scenarios are highlighted in appendix A.3.

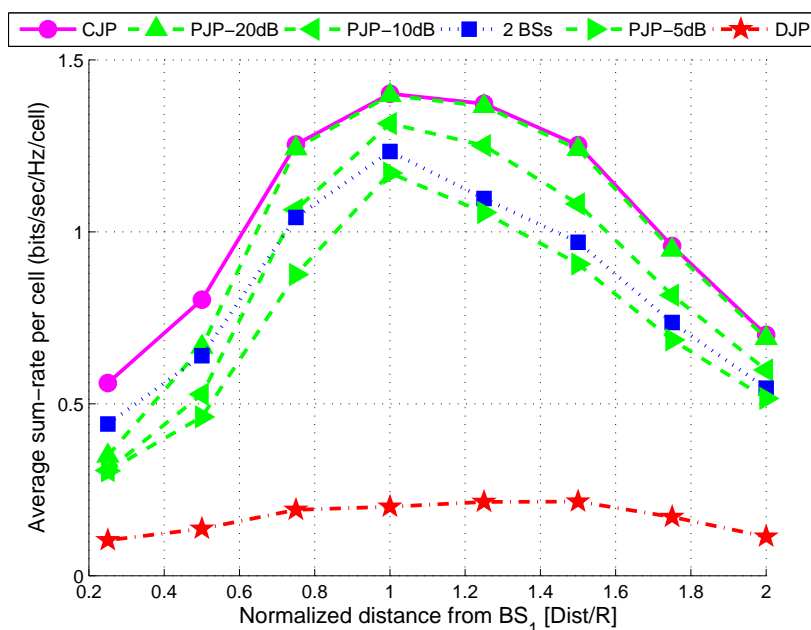


Figure 3.3: Average Sum-Rate per cell per RB for WINNER scenario B1 (NLOS) with 6 users, for non-adaptive frequency thresholding in PJP scheme.

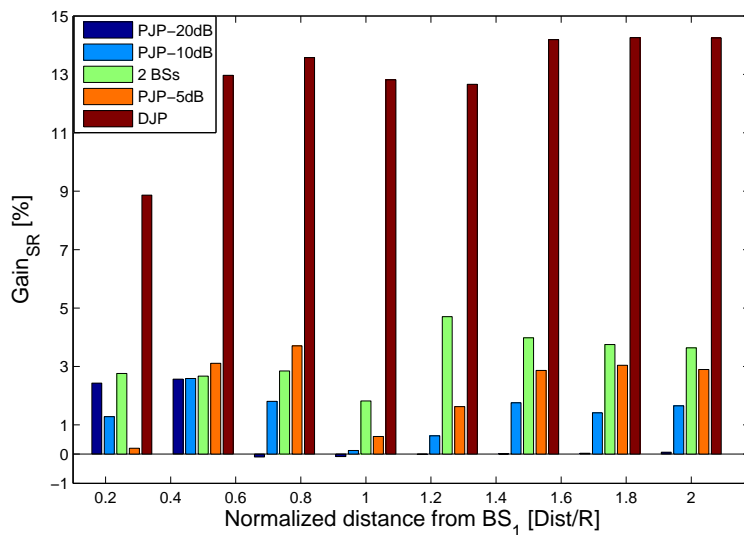


Figure 3.4: Percentage gain in average sum-rate per cell per RB due to frequency adaptive thresholding over non-adaptive frequency thresholding along the normalized distance from BS₁ for WINNER scenario B1.

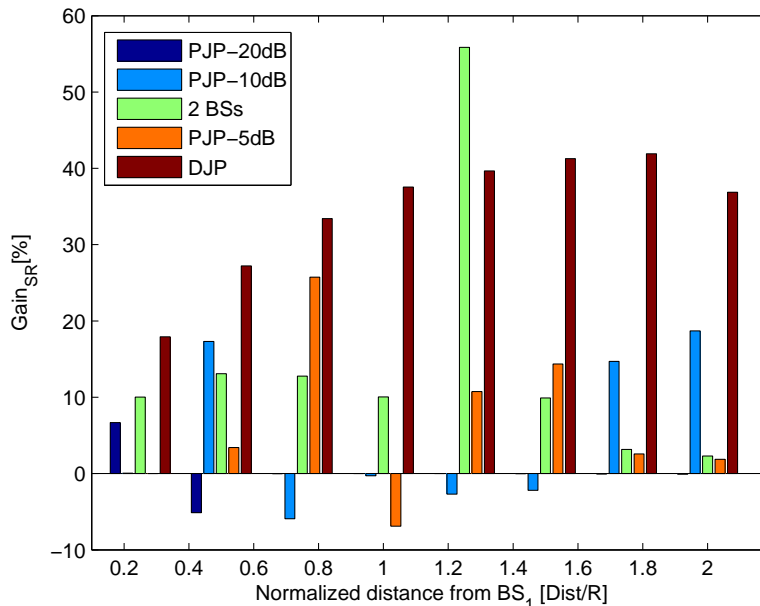


Figure 3.5: Percentage gain in average sum-rate per cell per RB due to frequency adaptive thresholding over non-adaptive frequency thresholding along the normalized distance from BS₁ for WINNER scenario C1.

3.5 Impact of Active links in PJP scheme

In Figure 3.6 a), we observe that the average number of BSs serving a user with frequency adaptive thresholding, \mathbf{T}^{FA} is lesser compared to the non-adaptive frequency thresholding, \mathbf{T}^{NA} . This is exemplified in Figure 3.6 b), where the relative average number of active links

$$R[\%] = \frac{\mathbf{T}^{FA} - \mathbf{T}^{NA}}{\mathbf{T}^{NA}}, \quad (3.2)$$

is evaluated along the normalized distance from BS₁. The negative values of the relative average clearly show that frequency adaptive thresholding achieves fewer active links, especially at the cluster-center ([Dist/R]=1) and the cell-edge ([Dist/R] ranging from 1.2 to 2). This leads to sparse channel matrices being available at the central unit for the design of ZF beamformer. Hence, an iterative partial zero-forcing beamformer based on [25, 26, 27] is justified.

3.6 Effect of rank deficient scaled channel correlation matrix

The scaled channel correlation matrix in equation (2.19) is said to be rank deficient when its rank is lesser than the number of users, i.e., $rank(\mathbf{Q}) < M$. Figure 3.7 depicts this condition along the normalized distance from BS₁. It

3.6. EFFECT OF RANK DEFICIENT SCALED CHANNEL CORRELATION MATRIX

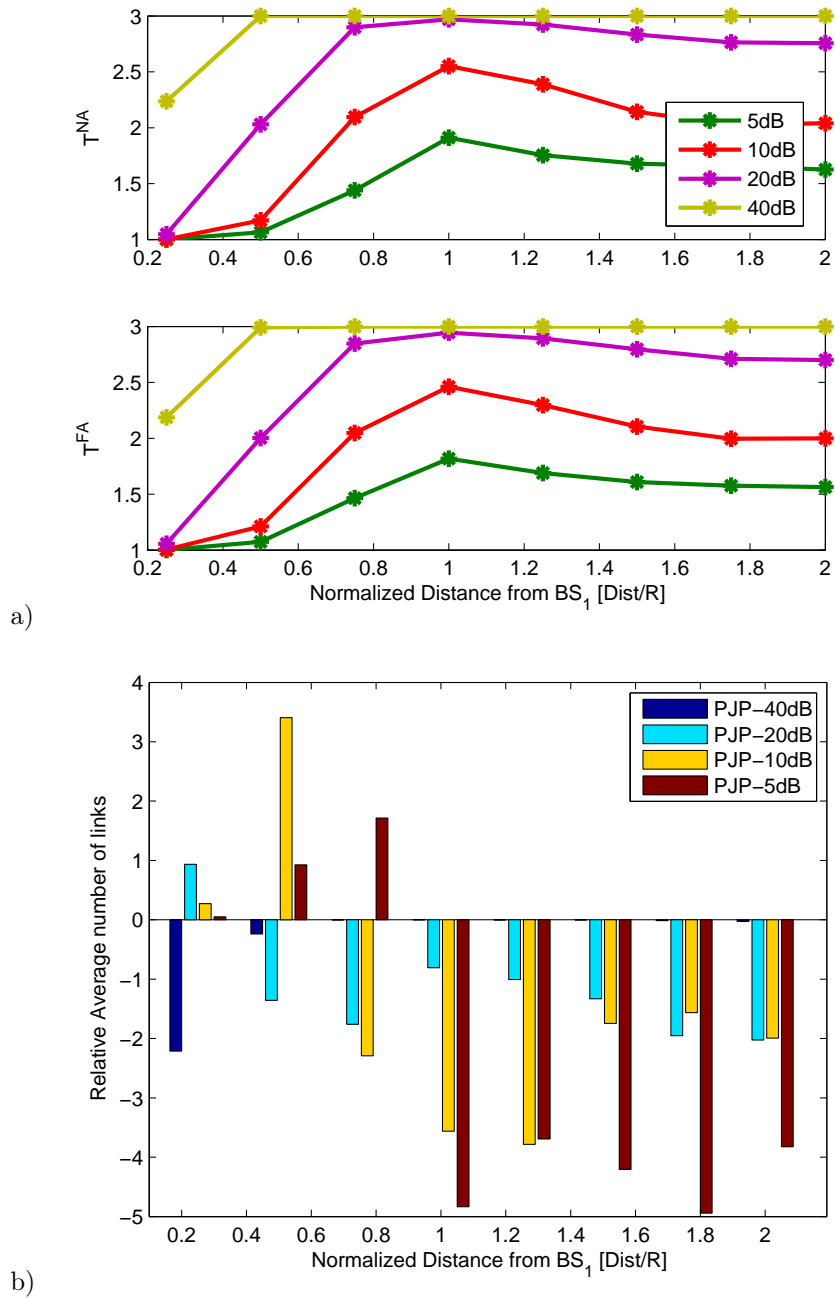


Figure 3.6: a) Average number of active links with non-adaptive frequency thresholding and frequency adaptive thresholding, b) Relative average number of active links of frequency adaptive thresholding versus non-adaptive frequency thresholding. Both figures are based on WINNER scenario B1.

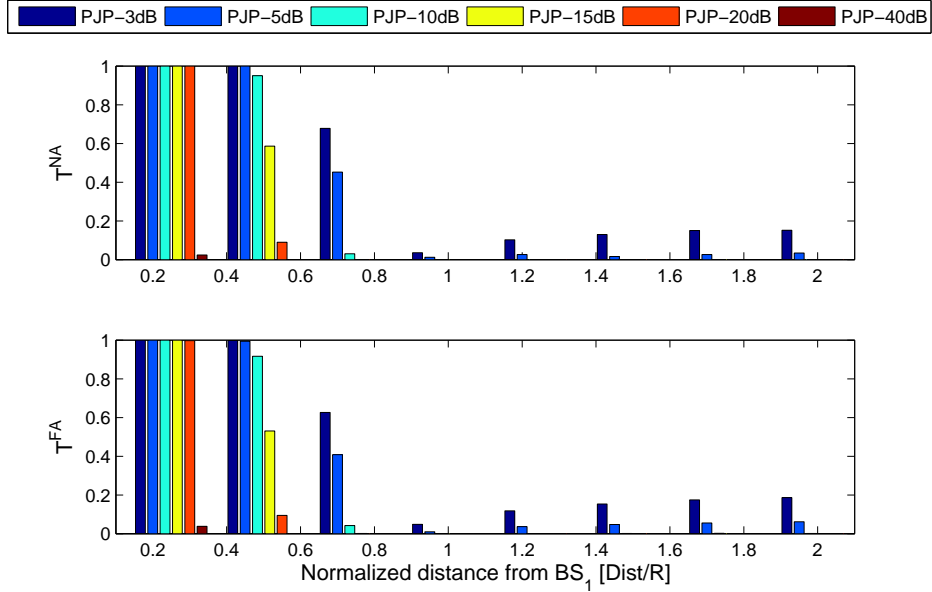


Figure 3.7: Probability that the scaled channel correlation matrix is rank deficient for the non-adaptive frequency thresholding and frequency adaptive thresholding in WINNER B1 (NLOS) scenario.

can be observed that the rank deficiency is more prominent near the BS_1 and for low values of active set threshold. This agrees with the results presented in [14], where the PJP with low values of the active set threshold did not achieve any gain with respect to the conventional single-BS case once the complexity requirements were taken into account. Figure 3.8 shows the difference between the rank deficiency of frequency adaptive thresholding with non-adaptive frequency thresholding, along the normalized distance from BS_1 . The appendix A.4 shows the rank deficiency encountered in other WINNER scenarios.

A *cooperation area* is defined based on the rank deficiency of the scaled channel correlation matrix, for a given active set threshold. For example, for PJP-10dB in Figure 3.7, the probability that the rank of the scaled channel correlation matrix tends zero is approximately at normalized distance greater than 0.7 from BS_1 . In Figure 3.9, the normalized distance of 0.7 from BS_1 corresponds to 1.8 BSs in average transmitting to a user. This forms a cooperation area based on the rank condition. The cooperation area for frequency adaptive thresholding and non-adaptive frequency thresholding are shown in Figure 3.9 a) and b). This approach is captured in Algorithm 3.1 where the matrix \mathbf{Q} is the scaled channel correlation matrix as defined in equation (2.19), the matrix \mathbf{G} is the channel energy scaling matrix given in equation (2.17) and the channel correlation matrix \mathbf{R} is given in equation (2.18).

In Figure 3.9, it is observed that the cooperation area is smaller with frequency adaptive thresholding than with non-adaptive frequency thresholding. It should be also be noted that this the cooperation area grows or shrinks with respective to the WINNER scenario as well. This is discussed in appendix A.5.

3.6. EFFECT OF RANK DEFICIENT SCALED CHANNEL CORRELATION MATRIX

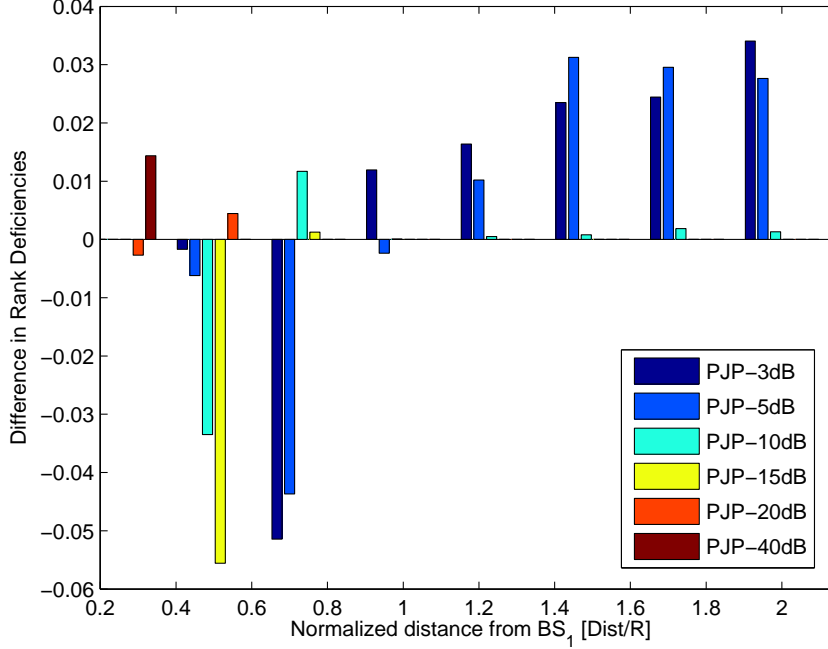


Figure 3.8: Rank deficiency is more prominent closer to BS₁ in non-adaptive frequency thresholding compared to frequency adaptive thresholding while it is vice-versa on the cell-edge in WINNER B1 (NLOS) scenario.

Algorithm 3.1 Definition of cooperation area for PJP

```

1: while  $M$  users in the cluster area do
2:   Users report CSI based on active set threshold
3:    $\mathbf{Q}_x \leftarrow (\mathbf{G}_x + \overline{\text{diag}}(\mathbf{R}_x))$ 
4:   if  $\text{rank}(\mathbf{Q}_x) = M$  then
5:     Full rank, users in cooperation area
6:     Use PJP,  $\mathbf{W}^x = \mathbf{U}_x^H \cdot (\mathbf{Q}_x)^{-1}$ 
7:   else
8:     Rank deficient, users not in cooperation area
9:     if active set threshold < 40 dB* then
10:      Increase the active set threshold, go to step 2
11:    else
12:      Use CJP or DJP schemes
13:    end if
14:  end if
15: end while

```

* An active set threshold value of 40dB results in all the BSs being active, i.e., CJP.

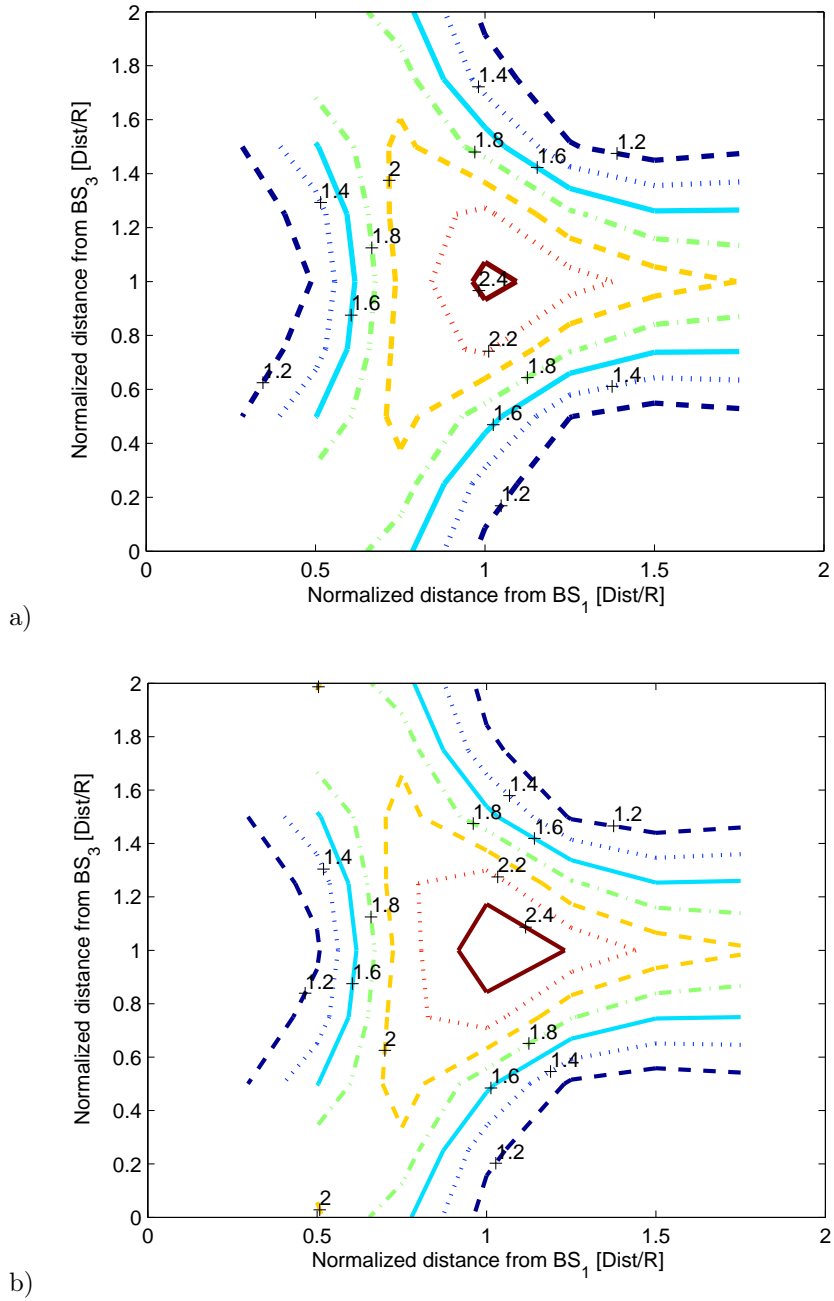


Figure 3.9: Cooperation Area for PJP-10dB for WINNER B1 (NLOS) scenario, a) frequency adaptive thresholding b) non-adaptive frequency thresholding.

Chapter 4

Conclusions and Future Work

The study of the JP algorithms in a frequency selective channel brought about an algorithm that can be used as a mechanism to trigger partial joint processing. When partial joint processing is unable to overcome the rank deficient conditions, the algorithm makes allowance to fallback on centralized joint processing or distributed joint processing. Hence, a Dynamic Coordinated MultiPoint scheme is achieved. The key results are briefly summarized below.

In a frequency selective channel, partial joint processing with frequency adaptive thresholding improves the average sum-rate up to 25% for a suburban macro-cell scenario. This gain comes at the cost of an increased user data exchange with respect to the non-adaptive frequency thresholding case. However, on an average less channel state information is fed back to the base stations.

On the other hand, the channel state information available at the transmitter side (central unit) to design the beamforming matrix is very limited and rank deficiency problems arise for low values of the active set thresholding and for users located close to the base station. To solve this problem, an algorithm is proposed that defines a cooperation area over the cluster, where the partial joint processing scheme can be performed via frequency adaptive or non-adaptive frequency thresholding for a given active set threshold value.

The extensions or the future work of this present framework consisting of the WINNER II channel model and the JP algorithms are highlighted below.

4.1 Weighted Power allocation in every Resource Block.

Presently, equal power allocation on all the RBs is performed. However, the power allocation can exploit the way in which the frequency adaptive thresholding and non-adaptive frequency thresholding are applied. A simple approach is a weighted power allocation, where the power available at the BS is non-equally allocated to the RB based on the channel conditions. Figure 4.1 shows a very coarse application of such power allocation, wherein every RB only the channel with the highest gain is considered. Different metrics can be considered to perform the weighted power allocation, such as the average energy in that RB.

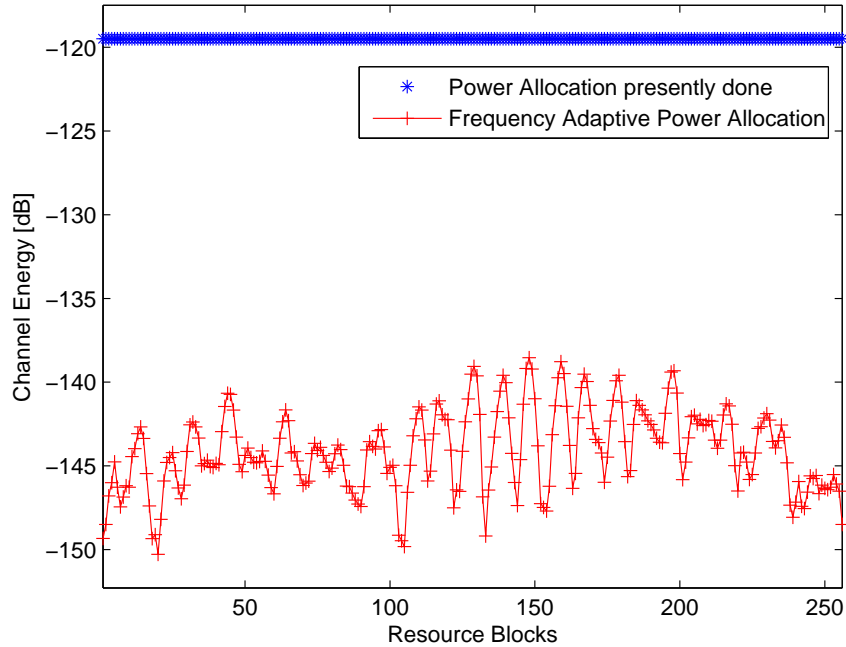


Figure 4.1: Power allocation based on channel conditions in every subcarrier or RB.

This approach should yield better performance of frequency adaptive thresholding compared to non-adaptive frequency thresholding.

4.2 Joint Processing for a set of OFDM carriers

Presently, only a single OFDM carrier/tone for each user is considered for JP in a RB. Hence, a set of OFDM frequencies/tones can be considered together for JP. This can be seen as being more aligned with the standards.

4.3 Hybrid thresholding

A hybrid two-step thresholding, combining the frequency adaptive and non-adaptive approaches, can reduce the backhaul cost with some performance degradation. This will be studied as part of our future work.

4.4 A realistic measure of the effects of imperfect CSI with Time evolution feature in WINNER channel model

Wei et al. [25] and Zhang et al. [28] model imperfect CSI as $\hat{\mathbf{H}} = \mathbf{H} + \mathbf{E}$, where \mathbf{H} is the channel matrix and \mathbf{E} is the channel error matrix, whose elements are i.i.d. complex Gaussian distributed with zero mean and variance $\sigma^2/2$ per real dimension. $\hat{\mathbf{H}}$ is the estimated channel matrix used for precoding and then transmitted over the present channel conditions \mathbf{H} . With the *Time Evolution* feature in the WINNER channel model, one can simulate the effects of delay (in sharing CSI between BSs), giving rise to CSI mismatch in a more realistic manner. Thus, quantifying the effects of delay with imperfect CSI. This might give more insight into the JP algorithms, as to how they are affected with imperfect CSI. Presently, with WIM2, the code seems to exist but this feature is disabled. Refer [19] for more details on *Time Evolution*.

4.5 Support for multiple antennas at MS

Presently, this framework has only support for single antenna MSs. This can be extended to multiple antennas, as future mobile devices are bound to have more than one antenna.

4.6 Antenna type

The focus on this thesis is more on the JP algorithms and CoMP specific antenna patterns are not yet been finalized in the literature. Nevertheless, the WINNER II Channel model gives room to specify an unique radiation pattern for every antenna being used. However, the 3GPP SCM [22] specifies antenna radiation patterns for MIMO, and this can be implemented with appropriate bore-sight configuration for the 3×1 MIMO links presented in this thesis.

4.7 Multi-WINNER scenario

The results presented in this thesis are confined to a given WINNER scenario. WINNER scenarios are developed based on extensive real life campaigns. For example, scenario B1-Urban micro-cell resembles a Manhattan grid and scenario A2 represents an indoor to outdoor. A more realistic scenario could be a more complex scenario which is a hybrid of B1 and A2. Such hybrid scenarios might give deeper understanding of the JP algorithms, especially when the users are separated by $2 \cdot \Delta x$ which is the diameter of the major axis of the elliptical curve, along which the users are randomly dropped.

Publication

© 2010 IEEE

Partial Joint Processing for Frequency Selective Channels

Tilak Rajesh Lakshmana*, Carmen Botella*, Tommy Svensson*, Xiaodong Xu[†], Jingya Li[†], Xin Chen[†]

*Signals and Systems, Chalmers University of Technology, Gothenburg, Sweden,
tilak@student.chalmers.se, {carmenb, tommy.svensson}@chalmers.se

[†]WTI Lab, Key Lab of UWC, Ministry of Education, Beijing University of Posts and Telecommunications, Beijing, China
{xuxiaodong, lijingya, chenxin}@mail.wtilabs.cn

Abstract—In this paper, we consider a static cluster of base stations where joint processing is allowed in the downlink. The partial joint processing scheme is a user-centric approach where subclusters or active sets of base stations are dynamically defined for each user in the cluster. In frequency selective channels, the definition of the subclusters or active set thresholding of base stations can be frequency adaptive (per resource block) or non-adaptive (averaged over all the resource blocks). Frequency adaptive thresholding improves the average sum-rate of the cluster, but at the cost of an increased user data interbase information exchange with respect to the non-adaptive frequency thresholding case. On the other hand, the channel state information available at the transmitter side to design the beamforming matrix is very limited and rank deficiency problems arise for low values of active set thresholding and users located close to the base station. To solve this problem, an algorithm is proposed that defines a cooperation area over the cluster where the partial joint processing scheme can be performed, frequency adaptive or non-adaptive, for a given active set threshold value.

I. INTRODUCTION

Coordinated MultiPoint (CoMP) schemes have been identified as one of the key technologies for mitigating intercell interference in future broadband communication systems [1], [2]. Under this framework, both coordinated beamforming and/or user scheduling and the more advanced joint processing between Base Stations (BSs) are included. In joint processing CoMP, multiple BSs can collaborate on the transmission and reception of user data. Under the assumption of perfect channel knowledge, perfect synchronization among BSs and negligible delays, the theoretical gains with joint processing CoMP are substantially larger than with coordinated beamforming. How much of these gains are preserved under more realistic assumptions is still an open issue. On the other hand, these larger performance gains come at the cost of an increased overhead in the system, since the amount of information exchanged between BSs and the required feedback from the users increase. To reduce this overhead, clustering of BSs is proposed. These techniques arrange clusters of BSs that may remain *static* in time, or may *dynamically* adapt to the changing conditions of the channel. Moreover, based on where the clustering decision is carried out, these approaches are further divided into *network-centric* or *user-centric*.

This work has been supported by The Swedish Agency for Innovation Systems (VINNOVA). The work has been performed in the framework of the Sino-Swedish program on ‘IMT Advanced and beyond’.

In the previous work [3], the performance of three joint processing schemes for the downlink of a static cluster of BSs was characterized and compared over a flat fading Rayleigh channel. In the Centralized Joint Processing (CJP) approach, global channel state information (CSI) was available at the transmitter side, and the BSs within the cluster jointly performed the power allocation and the design of the linear beamformer [1], [2]. With the aim of decreasing both the required interbase information exchange and feedback from the users, a Partial Joint Processing (PJP) scheme was evaluated, where different stages of joint processing between the BSs in the cluster were defined based on a user-centric clustering algorithm. Finally, a Distributed Joint Processing (DJP) scheme where the power allocation and the beamformers were locally calculated at each BS was also considered. In this last case, a multibase scheduling algorithm was required in order to assign users to BSs.

In this paper, we consider the impact over these joint processing schemes of a more realistic frequency selective fading channel using the WINNER II Channel Model [4]. Specifically, the problem of how to perform the PJP scheme arises¹. In the PJP scheme, each user in the cluster area is served by a user-centric *subcluster* or *active set* of BSs, which is defined based on an active set threshold value [3]. By doing this, the cluster becomes partially coordinated and different stages of joint processing are achieved. In the case of frequency selective channels, an OFDM-based approach can be considered where the active set thresholding is performed in every subcarrier or group of subcarriers, cf., Resource Block (RB) in 3GPP LTE [5]. This adaptive nature of forming the active set of BSs is referred in this paper as *frequency adaptive* thresholding. On the other hand, when the active set thresholding is performed over the entire channel without exploiting the frequency selectivity of the channel, we have *non-adaptive frequency* thresholding. With frequency adaptive thresholding, the subcluster of BSs transmitting to a user is defined within each RB. However, this implies that the subclusters of BSs for the user may change in each RB for a given time slot and that the benefit of the PJP scheme, i.e., the decreased amount of interbase information exchange, is no

¹Notice that a similar problem appears for the multibase scheduling technique required for the DJP scheme. However, in this paper, we focus on the PJP scheme.

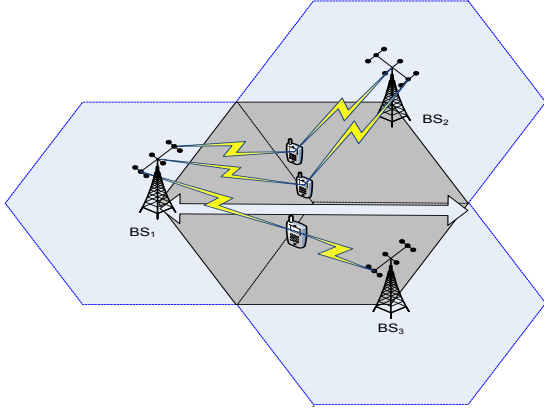


Figure 1. Cluster Layout. The shadowed hexagon is the cluster area under consideration.

longer possible, since all the user data needs to be available in each BS. In recent approaches involving clustering of sectors or BSs in frequency selective channels, this problem is solved by performing user grouping in a first step [6], and then allocating each group of users to a given RB. However, we are interested in the case where all the users are allocated to all the available RBs in each time slot, so that it is possible to take advantage of the frequency selectivity of the channel.

The outline of the paper is as follows. The system model for the CJP scheme is discussed in section II. The frequency adaptive and non-adaptive frequency thresholding for the PJP scheme are discussed in section III. As stated in [3], the PJP scheme introduces multiuser interference, since less CSI is available at the BSs for the design of the linear beamformer. In the scenario considered in the paper, the multiuser interference can even cancel the potential gains of the PJP scheme when the user is located close to the BS. Therefore, an algorithm is proposed in this section to define a cooperation area where the PJP scheme can be performed for a given active set threshold value. The simulation results are presented in section IV, and the contribution is concluded in section V.

II. SYSTEM MODEL

Consider the downlink of a cellular system with a given number of static clusters of BSs. Each static cluster is formed by K BSs with N_T antennas each, and M single antenna users (see Figure 1). The BSs within the cluster can cause intracluster interference due to overloading or loss of orthogonality in any dimension, and the transmissions from BSs outside this set give rise to intercluster interference.

In the worst case interference scenario and under a fairness assumption, the M users are allocated in all the RBs. In this case, the joint processing between BSs is implemented by joint linear beamforming and power allocation being applied in the frequency domain in every RB. Hence, the discrete-time received signal at the M users, $\mathbf{y} \in \mathbb{C}^{M \times 1}$, in a given RB of

the i th cluster can be expressed as²

$$\mathbf{y} = \mathbf{H}_i \mathbf{W}_i \sqrt{\mathbf{P}_i} \mathbf{x} + \mathbf{z}_{i'} + \mathbf{n}, \quad (1)$$

where $\mathbf{H}_i \in \mathbb{C}^{M \times KN_T}$ is the channel matrix, $\mathbf{W}_i \in \mathbb{C}^{KN_T \times M}$ is the beamforming matrix and $\sqrt{\mathbf{P}_i} \in \mathbb{R}^{M \times M}$ is the power allocation matrix. The transmitted symbols $\mathbf{x} \in \mathbb{C}^{M \times 1}$ are normalized to unit power and $\mathbf{z}_{i'}$ models the intercluster interference from all the $i' \neq i$ clusters. The receiver noise \mathbf{n} is spatially and temporally white, with a variance σ^2 , and is uncorrelated with the signals. The channel matrix \mathbf{H}_i is of the form

$$\mathbf{H}_i = [\mathbf{h}_{i,1}^T \mathbf{h}_{i,2}^T \dots \mathbf{h}_{i,M}^T]^T, \quad (2)$$

where $\mathbf{h}_{i,m} \in \mathbb{C}^{1 \times KN_T}$ is the channel from the m th user to all the BSs in the cluster. The beamforming matrix \mathbf{W}_i is

$$\mathbf{W}_i = [\mathbf{w}_{i,1} \mathbf{w}_{i,2} \dots \mathbf{w}_{i,M}], \quad (3)$$

where $\mathbf{w}_{i,m} \in \mathbb{C}^{KN_T \times 1}$ is the beamformer for the m th user. Considering the CSI from all the BSs in the i th cluster being available in the central unit for joint processing (CJP), the multiuser interference is canceled with a zero-forcing beamforming design, taking the pseudoinverse of \mathbf{H}_i

$$\mathbf{W}_i = \mathbf{H}_i^H (\mathbf{H}_i \mathbf{H}_i^H)^{-1}. \quad (4)$$

The intracluster interference is completely removed, i.e., $\mathbf{H}_i \mathbf{W}_i = \mathbf{I}_M$, where $\mathbf{I}_M \in \mathbb{R}^{M \times M}$ is an identity matrix, when $KN_T \geq M$ for the entire cluster [7]. At every BS, the maximum transmit power is restricted to P_{max} . Then, the power allocation matrix based on equal user power allocation [8] becomes

$$\sqrt{\mathbf{P}_i} = \left\{ \min_{k=1, \dots, K} \sqrt{\frac{P_{max}}{\|\mathbf{W}_i^k\|_F^2}} \right\} \cdot \mathbf{I}_M, \quad (5)$$

where \mathbf{W}_i^k are the rows of the matrix \mathbf{W}_i related to the k th BS. This power allocation is suboptimal, since it typically results in only one of the BSs meeting the maximum transmitted power requirement with equality, and hence, the remaining BSs transmit below the P_{max} value.

Assuming that the intercluster interference is effectively removed, the Signal to Interference Noise Ratio (SINR) at the m th user is

$$\text{SINR}_m = \frac{\|\mathbf{h}_{i,m} \mathbf{w}_{i,m}\|^2 p_{i,m}}{\sum_{\substack{j=1 \\ j \neq m}}^M \|\mathbf{h}_{i,m} \mathbf{w}_{i,j}\|^2 p_{i,j} + \sigma^2}, \quad (6)$$

²Notation: Boldface upper-case letters denote matrices, boldface lowercase letters denote vectors and italics denote scalars. Superscripts $(\cdot)^H$, $(\cdot)^T$ and $(\cdot)^{-1}$ stand for conjugate transpose, transpose and matrix inversion operations, respectively. We use $\mathbb{R}^{M \times N}$ and $\mathbb{C}^{M \times N}$ to denote the set of $M \times N$ real and complex matrices, respectively. $\mathbf{X}_{(i,j)}$ refers to the (i,j) th element of \mathbf{X} , whereas $\mathbf{X}_{(:,j)}$ and $\mathbf{X}_{(j,:)}$ indicate its j th column and j th row, respectively. The Frobenius norm of a matrix is denoted by $\|\cdot\|_F$. Finally, $\mathbb{E}\{\cdot\}$ denotes mathematical expectation.

where $p_{i,m} = (\sqrt{\mathbf{P}_{i(m,m)}})^2$. Assuming coherent combining at the receivers, the average sum-rate per cell achieved in the cluster area for a given RB becomes

$$SR_{RB} = \frac{1}{K} \mathbb{E}_H \left\{ \sum_{m=1}^M \log_2(1 + \text{SINR}_m) \right\}. \quad (7)$$

III. PARTIAL JOINT PROCESSING

The PJP algorithm is a threshold based window approach, where those BSs within the cluster whose links with the user fall within this window are included in the active set of the user and are allowed to cooperate. This window is a threshold level that is given by the cluster to the user. The user takes its best channel as its reference or serving BS link and sorts the links with the remaining BSs in the cluster relative to this reference link. This ordering is based on the channel strength or energy of the frequency selective channel, $\mathbf{h}_{i,m}(\tau; t)$ for the m th user, where τ is the tap delay in that time instant t . The PJP algorithm is a particular case of CJP and it asymptotically reaches the CJP performance when the active set threshold goes to infinity. Those BS links which fall within this given threshold are made active and those that fall outside this threshold are marked inactive. These active and inactive links are represented by ‘1’ and ‘0’, respectively, forming a *non-adaptive frequency* thresholding matrix, $\mathbf{T}^{NA} \in \{0, 1\}$ of size $[M \times K]$. Notice that $\mathbf{T}_{(m,k)}^{NA} = 1$ means that the link between the BS k in the cluster and the user m is active. In the non-adaptive frequency case, the active set thresholding is performed over an average of all the RBs. This active set of BSs is used in all the RBs but the user needs to feed back the CSI of these active links per RB.

With a realistic wideband channel, one can exploit the frequency selectivity by performing the active set thresholding in every RB. In this paper, this adaptive thresholding approach is called *frequency adaptive* thresholding. The frequency adaptive thresholding approach defines a \mathbf{T}^{FA} matrix in each RB. As a drawback, the active set of BSs may change in each RB. The backhauling load is increased, since the user data needs to be available in all the BSs of the cluster.

As we later show in the simulation results, frequency adaptive thresholding does improve the average sum-rate per cell per RB compared to the non-adaptive frequency thresholding, but at the cost of an increased user data exchange over the backhaul. With the PJP scheme, there is very limited CSI available for designing the beamformer, specially when the user is close to the BS and the active set threshold value is low. This motivates us to develop a partial zero-forcing beamformer based on the proposal in [9].

A. Partial Zero-Forcing Beamforming

The partial zero-forcing beamformer is derived in this section for both frequency adaptive and non-adaptive frequency thresholding approaches. The partial zero-forcing technique proposed in [9] is based on the definition of a useful matrix and interference matrices that modify the channel matrix to obtain useful and interference channel matrices. In our case,

\mathbf{T}^{NA} and \mathbf{T}^{FA} active link matrices are the basis for defining them. For a given time instant t , and considering the a th RB of the M users in the i th cluster, the useful channel matrix $\mathbf{U}_x \in \mathbb{C}^{M \times KN_T}$ is defined as

$$\mathbf{U}_x = [\mathbf{T}^x \otimes \mathbf{1}_{N_T}] \odot \mathbf{H}_i(f_a; t), \quad (8)$$

where \otimes is the Kronecker product, $\mathbf{1}_{N_T}$ is an all ones N_T row vector and \odot is the element-wise multiplication operation. x represents either TA or NA and f_a is the center frequency of the a th RB.

Using the active link matrices \mathbf{T}^{NA} and \mathbf{T}^{FA} , one can construct the matrices of the interference caused due to the transmission to the m th user in the cluster, $\mathbf{T}_{m,Int}^{NA}$ and $\mathbf{T}_{m,Int}^{FA}$, respectively. The rules for building the interference matrices for the m th user are that the data destined to the user only affects those users that share the transmitting BS. Such links that cause interference are marked ‘1’. Conversely, the inactive links for this user obviously do not cause interference to other users and also, the active links do not cause interference to itself. Hence, such links are marked ‘0’. The interference matrices try to remove the interference generated due to the transmission to a user by explicitly forcing this interference to zero. Therefore, the interference channel matrix $\mathbf{V}_{x,m} \in \mathbb{C}^{M \times KN_T}$ introduced by the transmission to the m th user in the i th cluster in the a th RB can be written as

$$\mathbf{V}_{x,m} = [\mathbf{T}_{m,Int}^x \otimes \mathbf{1}_{N_T}] \odot \mathbf{H}_i(f_a; t). \quad (9)$$

Assuming that the iterative partial zero-forcing algorithm proposed in [9] converges, the partial zero-forcing beamformer $\mathbf{W}_i^x \in \mathbb{C}^{KN_T \times M}$ is given by

$$\mathbf{W}_i^x = \mathbf{U}_x^H \cdot (\mathbf{G}_x + \overline{\text{diag}}(\mathbf{R}_x))^{-1}, \quad (10)$$

where $\overline{\text{diag}}(\cdot)$ are the off-diagonal elements of the matrix. The matrix $\mathbf{G}_x \in \mathbb{R}^{M \times M}$ is the channel energy scaling matrix given as $\mathbf{G}_x = \text{diag}(\mathbf{U}_x \mathbf{U}_x^H) \cdot \mathbf{I}_M$, where $\text{diag}(\cdot)$ are the diagonal elements of the matrix. The channel correlation matrix $\mathbf{R}_x \in \mathbb{C}^{M \times M}$ is given as

$$\mathbf{R}_x = \left(\mathbf{V}_{x,1} \mathbf{U}_{x(1,\cdot)}^H \cdots \mathbf{V}_{x,M} \mathbf{U}_{x(M,\cdot)}^H \right). \quad (11)$$

The partial zero-forcing beamformer can only be used when the scaled channel correlation matrix $\mathbf{Q}_x = [\mathbf{G}_x + \overline{\text{diag}}(\mathbf{R}_x)]$ is invertible. As we show in the simulation results, this condition is not always fulfilled, specially for low values of the active set threshold and users located close to a BS. Hence, we propose an algorithm to define a *cooperation area* for a given active set threshold value such that the frequency adaptive or non-adaptive PJP scheme can be performed.

B. Algorithm for Cooperation Area Definition

The algorithm for the definition of the cooperation area is based on the rank of the channel correlation matrix \mathbf{Q}_x .

Algorithm 1 Definition of cooperation area for PJP

```

1: while  $M$  users in the cluster area do
2:   Users report CSI based on active set threshold
3:   if  $\text{rank}(\mathbf{Q}_x) = M$  then
4:     Full rank, users in cooperation area
5:     Use PJP,  $\mathbf{W}_i^x = \mathbf{U}_x^H \cdot (\mathbf{G}_x + \text{diag}(\mathbf{R}_x))^{-1}$ 
6:   else
7:     Rank deficient, users not in cooperation area
8:     if active set threshold  $< 40$  dB* then
9:       Increase the active set threshold, go to step 2
10:    else
11:      Use CJP or DJP schemes
12:    end if
13:  end if
14: end while
  
```

* An active set threshold value of 40dB results in all the BSs being active, i.e., CJP.

IV. SIMULATION RESULTS

Consider a cluster of three BSs with three antennas each, spaced 4λ apart, and a cell radius of $R = 500$ m. $M = 6$ single antenna users are dropped at 8 predefined positions on the cluster layout (see the arrow in Figure 1), along a uniform distribution forming an ellipse around each position. The major and minor axis of the ellipse are $(2 \Delta x, 2 \Delta y)$, where $\Delta x \leq \frac{R}{16}$, $\Delta y \leq \frac{h/2}{16}$ and h is the height of the hexagon or cluster. A realistic frequency selective channel is simulated using the WINNER II channel model [4] (scenario B1, urban micro-cell, non-line of sight). 500 independent channel realizations in each predefined position are evaluated at 2GHz center frequency. The signal-to-noise ratio at the cell-edge (reference value for one user located at the cell-edge) is fixed to 15 dB. A 256-point Fast Fourier Transform is used, and one RB corresponds to one subcarrier.

Figure 2 shows the average sum-rate per cell per RB for the CJP, DJP and the PJP scheme with active set threshold values of 5, 10 and 20 dB, for the non-adaptive frequency thresholding approach. The 2 BSs case is a particular case of the PJP scheme, where always the best 2 BSs are transmitting to each user. The performance of the schemes is similar to [3]. Figure 3 shows the gain in the average sum-rate per cell per RB that can be achieved for the PJP scheme with frequency adaptive thresholding, i.e., $G_{SR}[\%] = \frac{SR^{FA} - SR^{NA}}{SR^{NA}}$. This gain depends on the scenario, e.g., for the PJP-5dB case, the maximum gain in the B1 scenario due to frequency adaptive thresholding is $\sim 3\%$, while $\sim 25\%$ is observed in case of scenario C1 (suburban macro-cell). It should also be pointed out that for high values of the active set threshold, PJP-20dB, there is no appreciable gain in the average sum-rate per cell per RB, since the partial zero-forcing beamformer cannot effectively remove the multiuser interference. The results for the DJP scheme confirm that the multibase scheduling technique presents a similar problem to the active set thresholding of the PJP scheme.

At the cluster center and for normalized distances from the BS₁ between 1.2 and 2, the average number of active links serving a user with frequency adaptive thresholding is

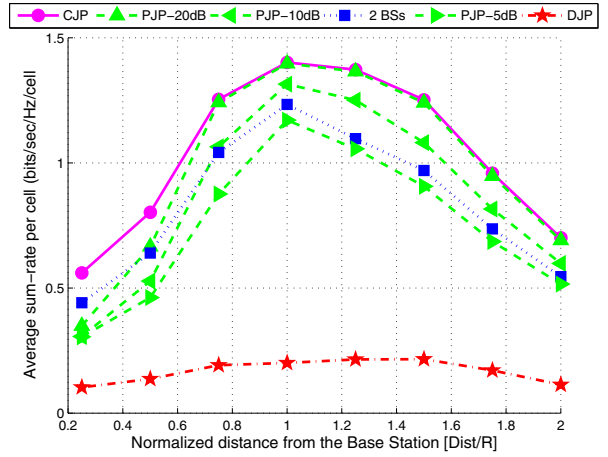


Figure 2. Average Sum-Rate per cell per RB vs. normalized distance from BS₁ when non-adaptive frequency thresholding is considered.

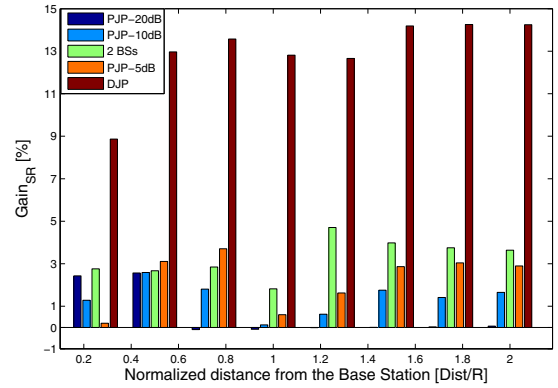


Figure 3. Percentage gain in average sum-rate per cell per RB due to frequency adaptive thresholding over non-adaptive frequency thresholding vs. normalized distance from BS₁.

less than with non-adaptive frequency thresholding. This is due to the fact that frequency adaptive thresholding is more sensitive to the threshold values as it quickly adapts to the frequency changes in every RB. The relative average number of active links, $R[\%] = \frac{\mathbf{T}^{FA} - \mathbf{T}^{NA}}{\mathbf{T}^{NA}}$, is illustrated in Table I. The negative values imply that with frequency adaptive thresholding, in average less CSI is fed back to the BSs. Notice that with frequency adaptive thresholding the user data invariably needs to be available at all the BSs, since the active set typically change along the RBs in a given time slot.

Rank deficiency problems of the scaled channel correlation matrix are more prominent close to BS₁ and for low values of the active set threshold, as shown in Figure 4 for the frequency adaptive case. This agrees with the results presented in [3], where the PJP with low values of the active set threshold did not achieve any gain with respect to the conventional single-BS case once the complexity requirements were taken into account. Applying the Algorithm 1 over the results in Figure 4, a *cooperation area* is defined for each value of the active

Table I
RELATIVE AVERAGE NUMBER OF ACTIVE LINKS OF FREQUENCY
ADAPTIVE THRESHOLDING VERSUS NON-ADAPTIVE FREQUENCY
THRESHOLDING

PJP-threshold	5dB	10dB	20dB	40dB
[Dist/R = 1]*	-4.84%	-3.56%	-0.81%	~ 0%
[Dist/R = 1.2 to 2]*	-4.16%	-2.27%	-1.57%	-0.01%
[Dist/R = 0.2 to 0.8]*	0.89%	0.46%	-0.72%	-0.82%

*Average values along the normalized distance from BS₁

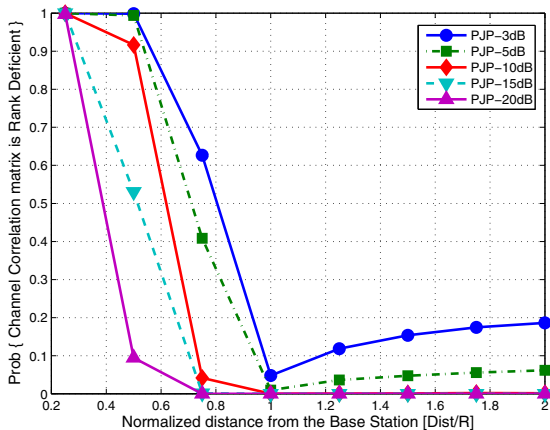


Figure 4. Rank deficiency of the scaled channel correlation matrix, \mathbf{Q}_x , is more prominent for users close to BS₁ and in the case of low values of the active set threshold. Results are shown for PJP schemes with frequency adaptive thresholding.

threshold, i.e., the PJP transmission is only allowed for that threshold value when the user is located in the cooperation area. When the outcome of the algorithm is that PJP is not feasible for any active set threshold value, the central unit switches to CJP or DJP schemes. It should be pointed out that for the same value of the active set threshold, the cooperation area due to frequency adaptive thresholding is smaller compared to non-adaptive frequency thresholding. Figure 5 shows the distribution of the average number of BSs transmitting to a user for the PJP-10dB. In this case, the cooperation area corresponds to more than 1.8 BSs transmitting to a user in average. On the other hand, the definition of the cooperation area identifies the cluster-edge users [10], where the use of intercluster coordination techniques is required in a multicell layout.

V. CONCLUSION

In a frequency selective channel, partial joint processing with frequency adaptive thresholding improves the average sum-rate up to 25% for a suburban macro-cell scenario. This gain comes at the cost of an increased user data exchange with respect to the non-adaptive frequency thresholding case. However, on an average less channel state information is fed back to the base stations. On the other hand, the channel state information available at the transmitter side to design the beamforming matrix is very limited and rank deficiency prob-

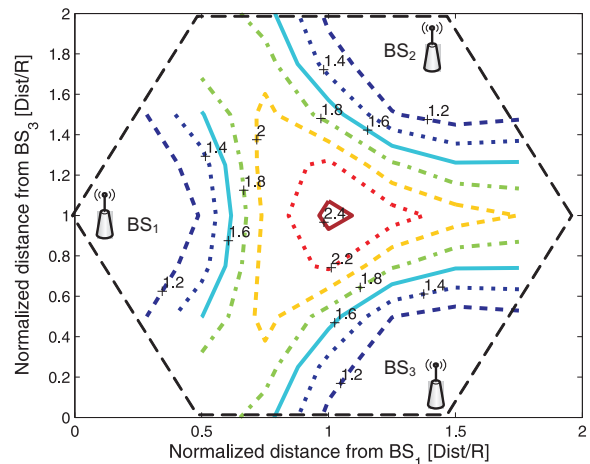


Figure 5. Distribution over the cluster area of the average number of BSs transmitting to one user for the PJP-10dB with frequency adaptive thresholding.

lems arise for low values of the active set thresholding and for users located close to the base station. To solve this problem, an algorithm is proposed that defines a cooperation area over the cluster, where the partial joint processing scheme can be performed via frequency adaptive or non-adaptive frequency thresholding for a given active set threshold value. A hybrid two-step thresholding, combining the frequency adaptive and non-adaptive approaches, can reduce the backhaul cost with some performance degradation. This will be studied as part of our future work.

REFERENCES

- [1] M.K. Karakayali, G.J. Foschini, R.A. Valenzuela, "Network coordination for spectrally efficient communications in cellular systems," *IEEE Wireless Communications*, vol. 13, no. 4, pp. 56-61, August 2006.
- [2] 3GPP TR 36.814-900, "3rd Generation Partnership Project; Technical Specification Group Radio Access Network; Further Advancements for E-UTRA Physical Layer Aspects (Release 9)," March 2010.
- [3] C. Botella, T. Svensson, X. Xu, H. Zhang, "On the performance of joint processing schemes over the cluster area," in *Proc. IEEE Vehicular Technology Conference*, May 2010.
- [4] P. Kyösti, J. Meilä, et al., "D1.1.2 WINNER II channel models: Part I channel models," IST-4-027756 WINNER II, September 2007.
- [5] E. Dahlman, S. Parkvall, J. Skold, P. Beming, "3G evolution: HSPA and LTE for mobile broadband," Second Edition, Academic Press, 2008.
- [6] L. Thiele, T. Wirth, M. Schellmann, Y. Hadisusanto, V. Jungnickel, "MU-MIMO with localized downlink base station cooperation and downtilted antennas," in *Proc. IEEE International Workshop on LTE Evolution*, June 2009.
- [7] Q. Spencer, A. Swindlehurst, M. Haardt, "Zero-forcing methods for downlink spatial multiplexing in multiuser MIMO channels," *IEEE Transactions on Signal Processing*, vol. 52, no. 2, pp. 461-471, February 2004.
- [8] H. Zhang and H. Dai, "Cochannel interference mitigation and cooperative processing in downlink multicell multiuser MIMO networks," *EURASIP Journal on Wireless Communications and Networking*, vol. 2, pp. 222-235, 2004.
- [9] X. Wei, T. Weber, A. Kuhne, A. Klein, "Joint transmission with imperfect partial channel state information," in *Proc. IEEE Vehicular Technology Conference*, April 2009.
- [10] J. Zhang, R. Chen, J. Andrews, A. Ghosh, R. Heath, "Networked MIMO with clustered linear precoding," *IEEE Transactions on Wireless Communications*, vol. 8, no. 4, pp. 1910-1921, April 2009.

Appendix

Appendix A

Interim results and more discussion

A.1 Base Station radiation pattern

For completeness, the total radiation pattern of a single BS with three antennas is depicted in the Figure A.1. This was generated using the MATLAB handbook of [29].

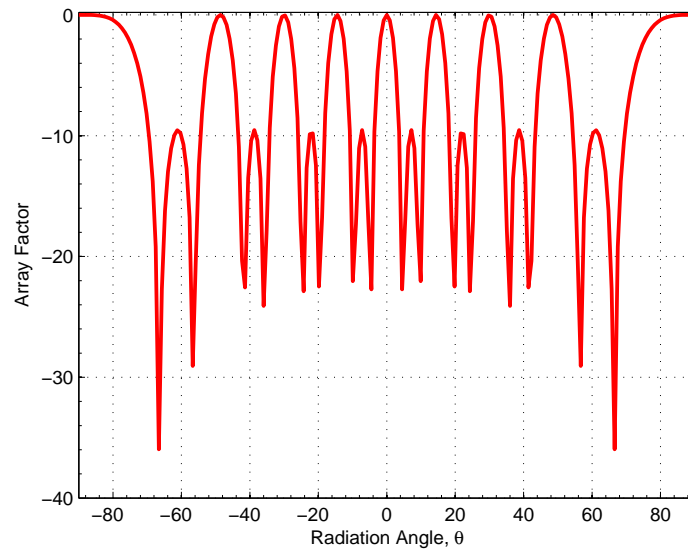


Figure A.1: Total Radiation pattern of a single BS with 3 antennas.

WINNER Scenario	Mean Square Error
A2 (Indoor to outdoor)	1.1665e-005
B1 (Urban micro-cell)	4.4566e-006
B2 (Bad urban micro-cell)	2.9785e-006
B4 (Outdoor to indoor)	1.6017e-006
C1 (Suburban macro-cell)	2.7769e-004
C2 (Urban macro-cell)	3.0218e-005

Table A.1: MSE between the average number of BSs serving a user with full channel statistics and the channel with only pathloss and shadow fading for various WINNER scenarios

A.2 Analysis of the active set threshold value

As seen in Figure 3.1, the average number of base stations serving a user in the PJP scheme depends on the active set threshold value. The WINNER scenario C1 in particular has a dip compared to other scenarios, due to the dominant LOS component in this scenario. This is confirmed when the WINNER scenarios are only configured for NLOS as shown in Figure A.2. Comparing a), b) and c), it can be inferred that the pathloss is the main ingredient that decides the average number of BSs transmitting to a user for a given threshold. This might seem obvious, as the shadow fading in WINNER is modeled as a log-normal distribution, whose standard deviation is fixed for a given scenario.

Figure A.3 shows the difference in the average number of BSs serving a user obtained with full channel statistics and with only pathloss and shadow fading for various WINNER scenarios. It can be observed that scenario C1 shows the biggest difference for active set threshold values ranging from 20 to 40 dB. This is most likely due to the dominant LOS in C1. Table A.1 shows the corresponding Mean Square Error (MSE) values. The difference in scenario C1 is not really significant. Hence, for the active set thresholding, the WINNER channel can be modeled as $\mathbf{H} = \sqrt{PL \cdot SF}$, with the pathloss and shadowing fading being derived from WINNER campaigns. Therefore, for users with low mobility, the long term channel statistics are good enough to define the active set of BSs in the PJP scheme. In this way, the feedback signaling is drastically reduced.

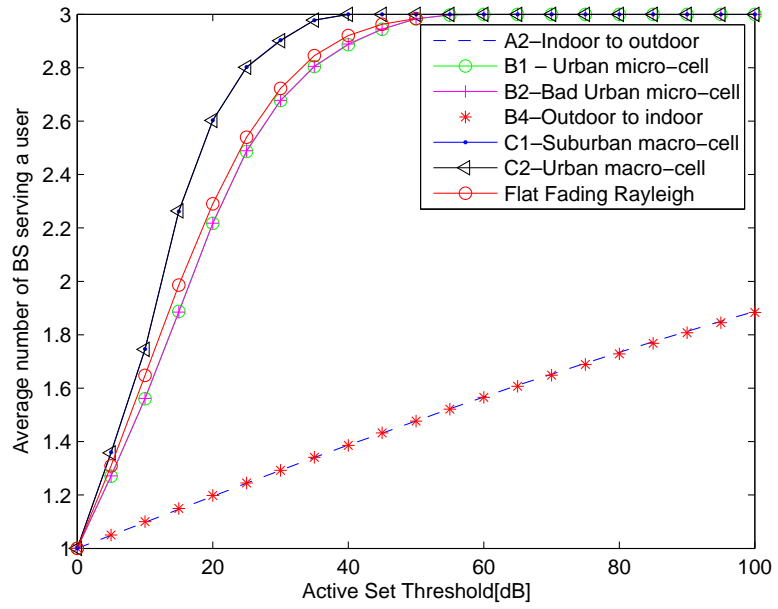
A.3 Sum-Rate plots of C1 and A2 WINNER scenarios

See Figure A.4 on page 51 and Figure A.5 on page 51 for the WINNER scenarios C1 and A2, respectively.

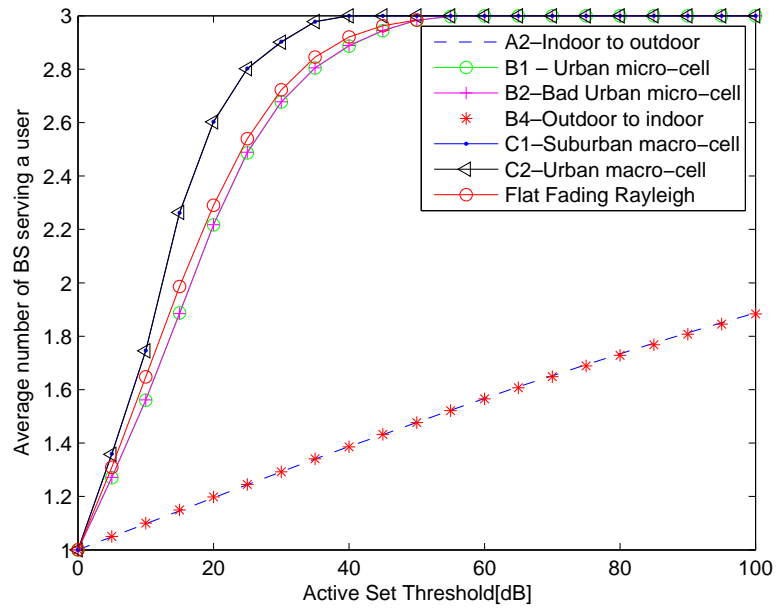
A.4 Rank deficiency in C1 and A2 WINNER scenarios

See Figure A.6 on page 52 for the WINNER scenarios C1 and A2. The algorithm 3.1 when applied for WINNER scenario A2 will probably result in

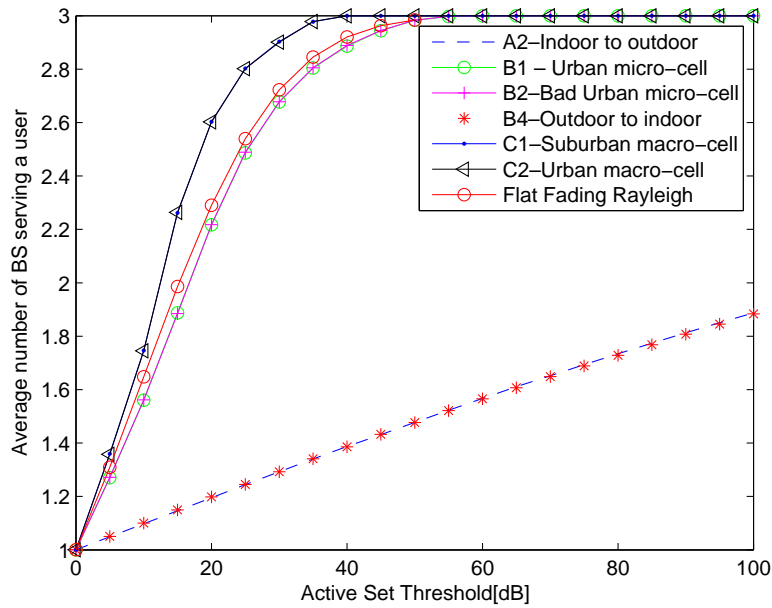
APPENDIX A. INTERIM RESULTS AND MORE DISCUSSION



a)



b)



c)

Figure A.2: Average number of BS serving a user for various WINNER (NLOS) scenarios considering a) full channel, b) only pathloss and shadow fading c) only pathloss.

choosing CJP or DJP, as even an active set threshold of 40 dB still shows rank deficiency throughout the normalized distance from BS₁.

A.5 Cooperation Area for C1 and A2 WINNER scenarios

In Figures A.7 and A.8, it can be observed that for a fixed PJP threshold of 10dB the cooperation area changes drastically for a given WINNER scenario. The cooperation area of frequency adaptive thresholding is smaller than non-adaptive frequency thresholding.

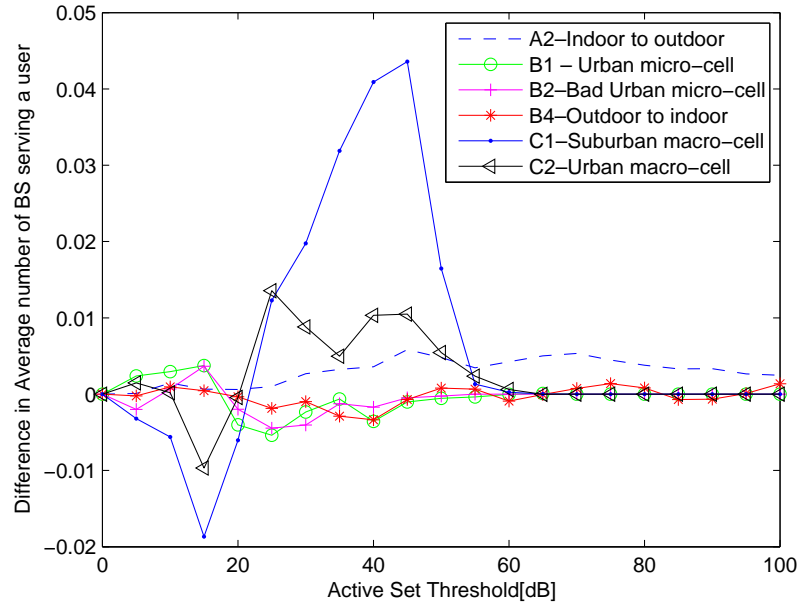
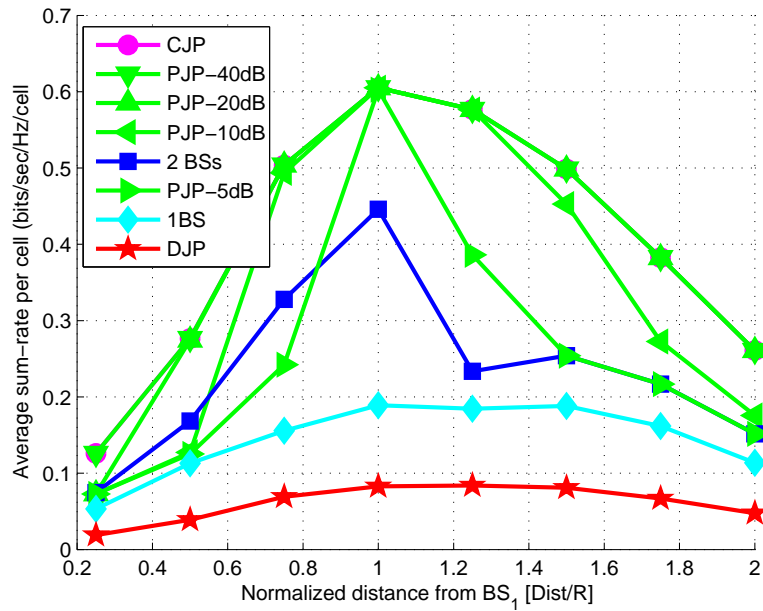
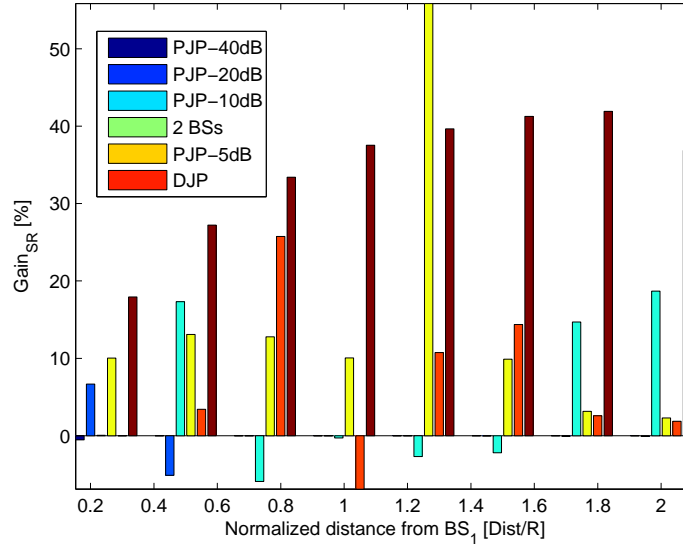


Figure A.3: Difference in the average number of BS serving a user between full channel and channel with only pathloss and shadow fading.



a)

A.5. COOPERATION AREA FOR C1 AND A2 WINNER SCENARIOS



b)

Figure A.4: WINNER Scenario C1 (NLOS) a) Average Sum-Rate per Cell per RB b) Percentage gain in average sum-rate per cell per RB due to Frequency adaptive thresholding compared to non-adaptive frequency thresholding.

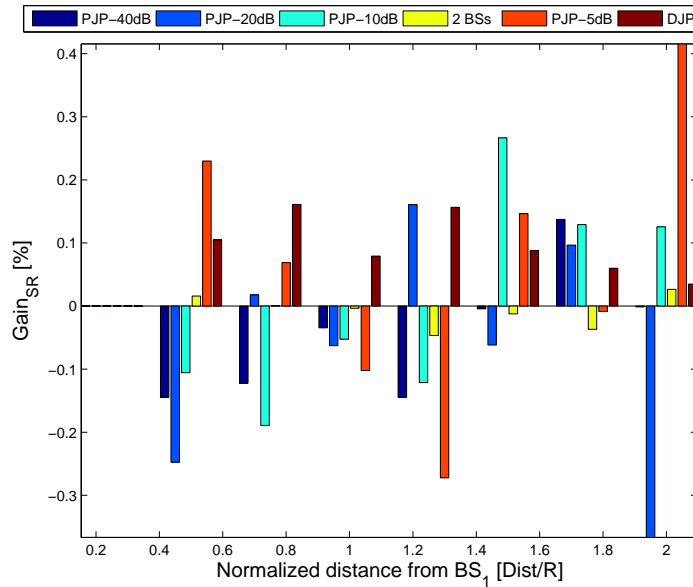


Figure A.5: WINNER Scenario A2 (NLOS), percentage gain in average sum-rate per cell per RB due to Frequency adaptive thresholding compared to non-adaptive frequency thresholding.

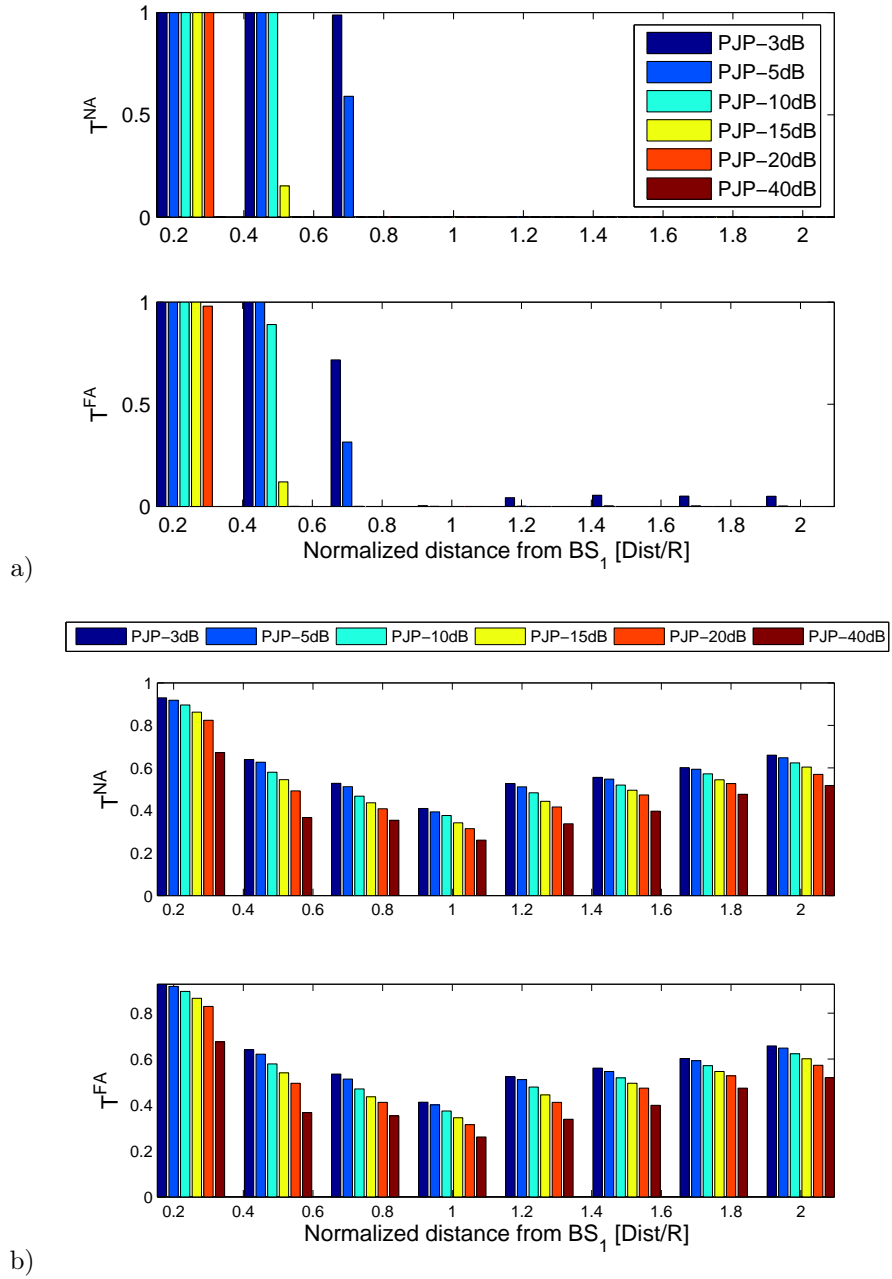
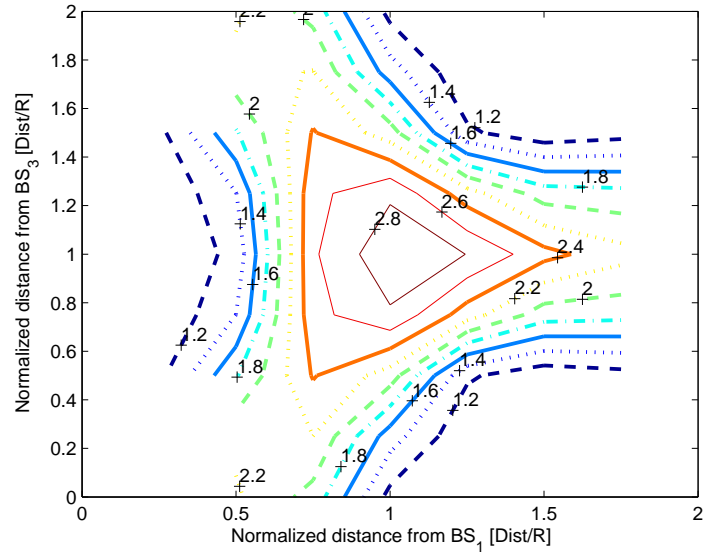
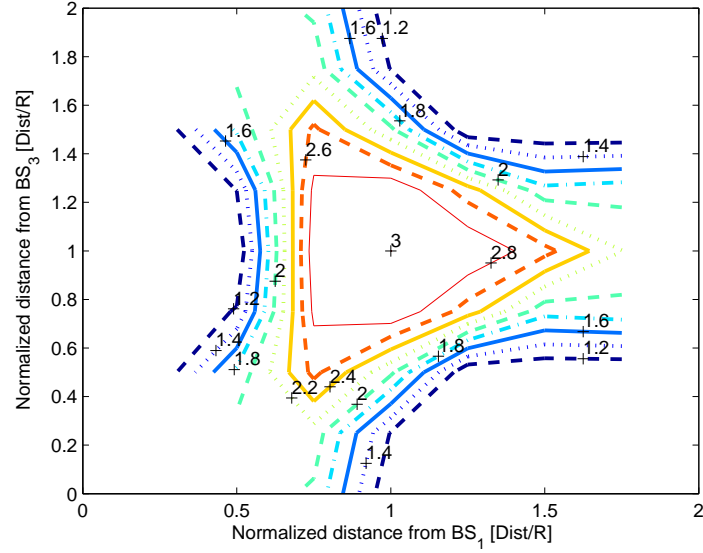


Figure A.6: WINNER Scenarios (NLOS) a) C1, the rank deficiency is only prominent close to the BS and b) A2, the rank deficiency exists even for high thresholds.

A.5. COOPERATION AREA FOR C1 AND A2 WINNER SCENARIOS



a)



b)

Figure A.7: Cooperation area for PJP-10dB for WINNER scenarios C1 (NLOS), a) frequency adaptive thresholding and b) non-adaptive frequency thresholding.

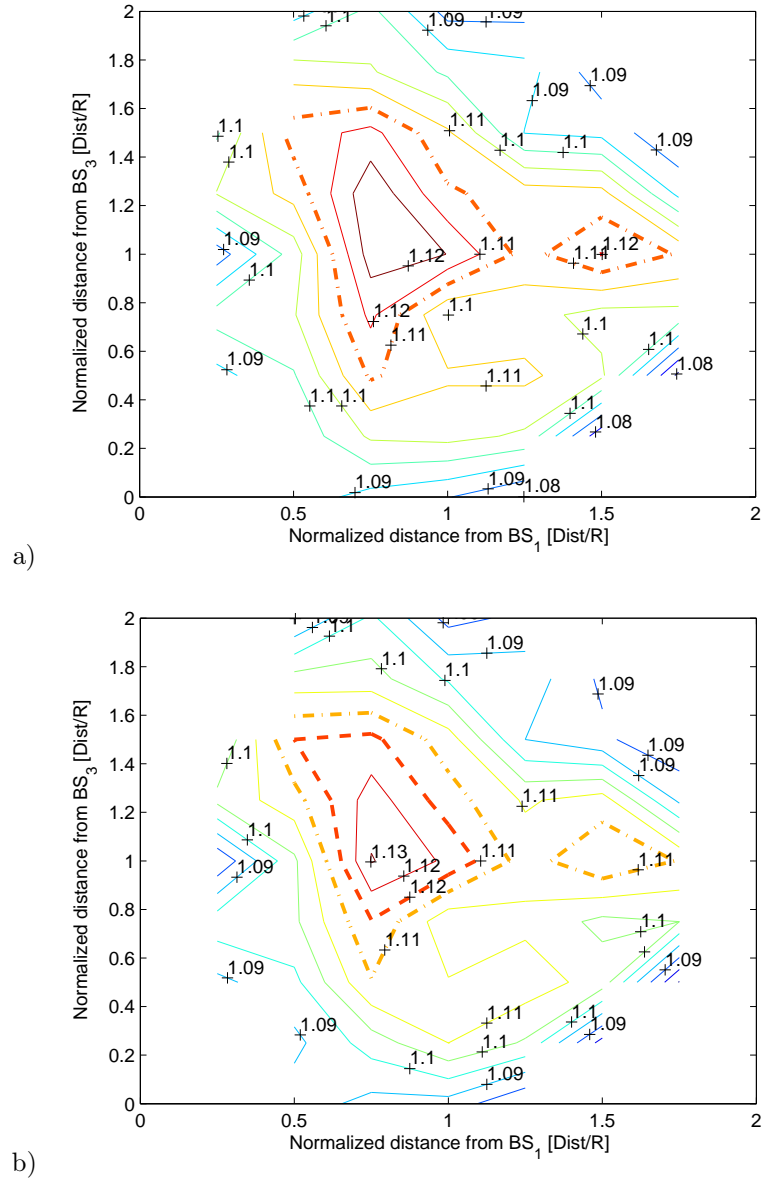


Figure A.8: Cooperation area for PJP-10dB for WINNER scenarios A2 (NLOS), a) frequency adaptive thresholding and b) non-adaptive frequency thresholding.

Appendix B

MATLAB details

Initial execution times were in days and the worst case being weeks for 12 users which is quite an overhead to quickly try out new ideas. Apart from this, the volume of data generated for 3, 6, 9 and 12 users for all the 54 grid positions with 500 channel realizations at each position, is nearly 15, 30, 45 and 60 gigabytes, respectively. Hence, there is a need to reduce these execution times and manage the data logs efficiently. Even doing a simple job of transferring these logs from the C³SE simulation cluster to the local 1 tera-byte hard disk can be cumbersome. This appendix deals with how these issues are addressed in a reasonably efficient way.

File Size: Saving the MATLAB workspace variables in .mat files in terms of ~ 10 kilo-bytes is useless. For now, the file system access is the bottleneck when reading/writing or deleting files. Having a file size greater than 5 megabytes, might cause potential loading problems, as MATLAB compresses the file before saving it. Thus, for loading them, MATLAB needs to decompress it which takes a long time (depending on the processor and the available RAM). Hence, my recommendation is to save files of size $>500\text{KB}$ and $<5\text{MB}$.

File Transfer: Transferring such giga-bytes of data from the simulation cluster to the local computer can be a huge task. A basic File Transfer Protocol (FTP) is slow and even an automatic triggering of such file transfer is slow. FileZilla is a free FTP software that intelligently transfers data from the source directory to the destination directory. This tool can be configured to have a maximum of ten sFTP links simultaneously. This drastically reduces the file transfer time. Presently, the only drawback is that FileZilla does not support command line options to trigger these transfers automatically.

B.1 Parallel Computing Toolbox

When the MathWorks Parallel Computing Toolbox license for distributed computing is not available, the only possible way to use the Parallel Computing Toolbox is locally. Hence, only a node consisting of four cores can be requested. The grid positions or locations can be chosen to run in parallel. A *parfor*

(*parallel for*) loop is used for this purpose. The *parfor* takes every loop iteration and runs them parallelly. With four core (CPU) machine, four loops are executed simultaneously. Hence, the execution time is drastically reduced by a factor of four compared to a single core simulation. The MATLAB code below shows how to use *parfor*. Typically, the outermost *for* loop is parallelized using *parfor*. When running multiple *parfor* jobs on the cluster, one has to specify the "*sched.DataLocation*". This will make sure that every parallel job submitted has a unique space where MATLAB stores its internal data for parallel processing. As per MATLAB support, this will avoid errors like: "*Failed to create and submit a parallel job. This is caused by: A parallel job must contain 1 task prior to submission*". The MATLAB pseudocode is given in Algorithm B.1.

Some drawbacks: The entire simulation is contained under one simulation. Any failure on the cluster machine where this code is executing will potentially lose all the data. The iterations for the *parfor* loop need to be in increasing order and a vector of different locations cannot be specified. These drawbacks are overcome using Single Core computing Section B.3.

Algorithm B.1 MATLAB pseudocode when using *parfor*

```
% Configure the location for the local scheduler data
% when using multiple parfor jobs simultaneously
if (exist('local_scheduler_data','dir') == 0)
    mkdir local_scheduler_data
end
sched=findResource('scheduler','type','local');
sched.DataLocation = strcat(pwd,'/local_scheduler_data');

% Actual parallel processing begins here
matlabpool
parfor location = 1:54
    % Example: Monte Carlo type simulation
    % parfor is typically used on the outermost for loop
end
matlabpool close
```

B.2 *deploytool*

A standalone application can be built using MATLAB Compiler Runtime (MCR) that can be launched as a console application independent of MATLAB, i.e., royalty free, then the *deploytool* is a good option. Moreover, the executable generated is independent of any MATLAB license, which is crucial when running on the cluster as the simulation can be terminated if the license is not available. The availability of license is a potential pitfall when running on the cluster, as they are easily exhausted. Hence, *deploytool* becomes a very attractive option. One of the main intentions of using this was to see if there are benefits in speeding up the computations while simultaneously using *parfor*. This was not explored further as it was an overhead to compile a project and another simpler technique of distributing the computations was more convenient. This is described in the next section.

B.3 How to efficiently run simulations on the Cluster (Single Core)

Typically, the cluster is mostly loaded between 97-99%. At most, one can easily find a single core somewhere on the cluster that is not used. The program was modularized such that it was specific to one position on the grid, i.e., 54 (positions) independent simulations can be run simultaneously, with each simulation demanding a single core instead of four cores. This way, one can easily avoid being stuck in the queue. This approach can be viewed as distributed computing, where the results are collated from the .mat files saved from these individual runs. One of the most important aspects of this approach is that the execution time is reduced to the time taken by one grid position with 500 channel realizations, i.e., all the 54 positions can be launched simultaneously. To quickly get the job from queued state to the running state, one should evaluate the conditions on the cluster and the latest rules of C³SE.

A summary of the execution time is captured in Table B.1.

Execution Time (hr:min)	<i>parfor</i>	<i>deploytool</i>	single core
3 users	12	N/A	~ 0 : 45
6 users	24	N/A	~ 1 : 30
9 users	36	N/A	2 : 15*
12 users	48	N/A	3 : 00*

* denotes extrapolated value and N/A - Not Available

Table B.1: Summary of Execution Time

Apart from this, sections of the code that either consume a lot of time or use the MATLAB license can be avoided, especially if they remain static throughout the simulation. They can be simply stored one time as a .mat file and retrieved whenever needed. This is useful, for example, to create an antenna array from WIM2, which consumes a lot of time. As the antenna radiation pattern is fixed, only the beamformers tune them, they can be stored as a .mat file. Also, the generation of the uniform distribution of users around an ellipse at a grid point, presently uses Spline Toolbox and hence, consumes this MATLAB license and execution time. When the license is not available, this can kill the simulation. Hence, storing the one-time generated data as a .mat file can mitigate these time consuming sections of the code and avoid the license overhead.

Bibliography

- [1] E. Agrell, “The structure of a technical report,” September 2009, rev 4.1.
- [2] S. Parkvall and D. Astely, “The Evolution of LTE towards IMT-Advanced,” *Journal of Communications*, vol. 4, no. 3, 2009. [Online]. Available: <http://academypublisher.com/ojs/index.php/jcm/article/view/0403146154>
- [3] M. Karakayali, G. Foschini, and R. Valenzuela, “Network coordination for spectrally efficient communications in cellular systems,” *Wireless Communications, IEEE*, vol. 13, no. 4, pp. 56–61, August 2006.
- [4] “Coordinated Multi-Point Transmission in LTE-Advanced Downlink-Test system,” Press Report, Deutsche Telekom and Fraunhofer Institute for Communications, Heinrich-Hertz Institute (HHI), July 2009. [Online]. Available: http://www.easy-c.de/pm_090708.pdf
- [5] M. Costa, “Writing on dirty paper,” *IEEE Transactions on Information Theory*, vol. 29, no. 3, pp. 439–441, 1983.
- [6] T. Yoo and A. Goldsmith, “On the optimality of multiantenna broadcast scheduling using zero-forcing beamforming,” *IEEE Journal on Selected Areas in Communications*, vol. 24, no. 3, pp. 528–541, 2006.
- [7] H. Zhang and H. Dai, “Cochannel interference mitigation and cooperative processing in downlink multicell multiuser MIMO networks,” *EURASIP Journal on Wireless Communications and Networking*, vol. 2004, no. 2, pp. 222–235, 2004.
- [8] G. Freisen, “4G backhaul options: Evaluating key requirements a must for operators,” February 2010. [Online]. Available: http://www.telecomengine.com/article.asp?HH_ID=AR_6187
- [9] G. J. Foschini and M. J. Gans, “On limits of wireless communications in a fading environment when using multiple antennas,” *Wireless Personal Communications*, vol. 6, no. 3, pp. 311–335, 1998.
- [10] 3GPP TR 36.814-900, “3rd Generation Partnership Project; Technical Specification Group Radio Access Network; Further Advancements for E-UTRA Physical Layer Aspects (Release 9),” March 2010.
- [11] M. Boldi, C. Botella, F. Boccardi, V. D’Amico, E. Hardouin, M. Olsson, H. Pennanen, P. Rost, V. Savin, T. Svensson and A. Tölli, “D1.8 Intermediate Report on CoMP (Coordinated Multi-Point) and Relaying

BIBLIOGRAPHY

- in the Framework of CoMP,” CELTIC CP5-026 WINNER+, November 2009. [Online]. Available: <http://projects.celtic-initiative.org/WINNER+>
- [12] “Network MIMO: Coherently-Coordinated Base Stations,” Alcatel-Lucent Bell Labs, December 2008. [Online]. Available: <http://innovationdays.alcatel-lucent.com/2008/documents/Network%20MIMO.pdf>
- [13] H. Bölcskei, D. Gesbert, C. B. Papadias, and A. J. van der Veen, *Space-Time Wireless Systems, From Array Processing to MIMO Communications*. Cambridge University Press, 2006.
- [14] C. Botella, T. Svensson, X. Xu, and H. Zhang, “On the performance of joint processing schemes over the cluster area,” in *IEEE Proceedings Vehicular Technology Conference*, May 2010.
- [15] E. Dahlman, S. Parkvall, J. Skold, and P. Beming, *3G evolution: HSPA and LTE for mobile broadband*. 2nd edition, Academic Press, 2008.
- [16] Q. Spencer, A. Swindlehurst, and M. Haardt, “Zero-forcing methods for downlink spatial multiplexing in multiuser MIMO channels,” *IEEE Transactions on Signal Processing*, vol. 52, no. 2, pp. 461–471, February 2004.
- [17] International Telecommunication Union, “ITU-R M.2134: Requirements related to technical performance for IMT-Advanced radio interface(s),” 2008.
- [18] M. Narandzic, M. Kaske, C. Schneider, M. Milojevic, M. Landmann, G. Sommerkorn, and R. Thoma, “3D-Antenna Array Model for IST-WINNER Channel Simulations,” in *IEEE 65th Vehicular Technology Conference*, April 2007, pp. 319–323.
- [19] P. Kyösti, et al., “IST-WINNER D1.1.2, ver 1.1, WINNER II Channel Models,” September 2007. [Online]. Available: <https://www.ist-winner.org/WINNER2-Deliverables/D1.1.2v1.1.pdf>
- [20] L. Hentilä, P. Kyösti, M. Käske, M. Narandzic and M. Alatosava, “MATLAB implementation of the WINNER Phase II Channel Model, ver1.1,” December 2007. [Online]. Available: http://projects.celtic-initiative.org/winner+/phase_2_model.html
- [21] L. Thiele, M. Schellmann, T. Wirth, V. Jungnickel, F. Boccardi, and H. Huang, “DFT-based vs. cooperative MET-based MU-MIMO in the downlink of cellular OFDM systems,” in *International ITG Workshop on Smart Antennas*, 2009.
- [22] 3GPP TR 25.996, “3rd Generation Partnership Project; Technical Specification Group Radio Access Network; Spatial channel model for MIMO simulations (Release 6).”
- [23] V. Jungnickel, L. Thiele, T. Wirth, T. Haustein, S. Schiffermuller, A. Forck, S. Wahls, S. Jaeckel, S. Schubert, H. Gabler, C. Juchems, F. Luhn, R. Zavratak, H. Droste, G. Kadel, W. Kreher, J. Mueller, W. Stoermer, and G. Wannenmacher, “Coordinated multipoint trials in the downlink,” in *GLOBECOM Workshops*, December 2009.

- [24] H. Skjevling, D. Gesbert, and A. Hjørungnes, “Low-complexity distributed multibase transmission and scheduling,” in *EURASIP Journal on Advances in Signal Processing*, Volume 2008, Article ID 741593, 2008.
- [25] X. Wei, T. Weber, A. Kuhne, and A. Klein, “Joint transmission with imperfect partial channel state information,” in *Vehicular Technology Conference*, April 2009.
- [26] X. Wei, T. Weber, A. Ahrens, and S. Deng, “Decentralized interference management in mobile radio networks,” *Frequenz*, vol. 61, no. 11-12, pp. 259–269, 2007.
- [27] X. Wei, T. Weber, A. Wolfgang, and N. Seifi, “Joint Transmission with Significant CSI in the Downlink of Distributed Antenna Systems,” in *IEEE International Conference on Communications*, 2009.
- [28] J. Zhang, R. Chen, J. Andrews, A. Ghosh, and R. Heath, “Networked MIMO with clustered linear precoding,” *IEEE Transactions on Wireless Communications*, vol. 8, no. 4, pp. 1910–1921, April 2009.
- [29] P. S. Kildal, *Foundations of Antennas: A Unified Approach for Line-of-Sight and Multipath*. Studentlitteratur, 2009.